Optical Phased Array Technology

PAUL F. MCMANAMON, SENIOR MEMBER, IEEE, TERRY A. DORSCHNER, MEMBER, IEEE, DAVID L. CORKUM, LARRY J. FRIEDMAN, MEMBER, IEEE, DOUGLAS S. HOBBS, MICHAEL HOLZ, SERGEY LIBERMAN, HUY Q. NGUYEN, DANIEL P. RESLER, RICHARD C. SHARP, MEMBER, IEEE, AND EDWARD A. WATSON

Optical phased arrays represent an enabling new technology that makes possible simple, affordable, lightweight, optical sensors offering very precise stabilization, random-access pointing, programmable multiple simultaneous beams, a dynamic focus/defocus capability, and moderate to excellent optical power handling capability. These new arrays steer or otherwise operate on an already formed beam, as compared to modern microwave phased arrays which both generate a beam and direct it in a specific direction. A phase profile is imposed on an optical beam as it is either transmitted through or reflected from the phase shifter array. The imposed phase profile steers, focuses, fans out, or corrects phase aberrations on the beam. The array of optical phase shifters is realized through lithographic patterning of an electrical addressing network on the superstrate of a liquid crystal waveplate. Refractive index changes sufficiently large to realize full-wave differential phase shifts can be effected using low (<10 V) voltages applied to the liquid crystal phase plate electrodes. High efficiency large-angle steering with phased arrays requires phase shifter spacing on the order of a wavelength or less; consequently addressing issues make 1-D optical arrays much more practical than 2-D arrays. Orthogonal oriented 1-D phased arrays are used to deflect a beam in both dimensions. Optical phased arrays with apertures on the order of 4 cm by 4 cm have been fabricated for steering green, red, 1.06 μm, and 10.6 μm radiation. Steering efficiencies of about 60% at 4° and 85% at about 2° have been achieved to date with switching times as short as a few milliseconds in the visible. Fluences of several hundred W/cm^2 have been demonstrated at 10.6 μm with nonoptimally engineered devices. Higher fluences can be handled at shorter wavelengths. Larger apertures are feasible, as is operation at other wavelengths and significantly faster switching times. System concepts that include a passive acquisition sensor as well as a laser radar are presented.

Manuscript received June 30, 1995; revised November 14, 1995. This work was supported in part by Raytheon internal funds, and in part by the Air Force Wright Laboratory at Wright Patterson AFB, Dayton, OH.

P. F. McManamon and E. A. Watson are with Wright Laboratory, Wright Patterson AFB, OH 45433 USA.

D. L. Corkum is with Texas Instruments, Attleborough, MA 02703 USA.

T. A. Dorschner, L. J. Friedman, D. S. Hobbs, M. Holz, D. P. Resler, and R. C. Sharp are with Raytheon Company, Electronic Systems, Lexington, MA 02173 USA.

H. Q. Nguyen is with Kopin Corp., Taunton, MA 02173 USA.

S. Liberman is with SemiTest, Billerica, MA 01821 USA.

Publisher Item Identifier S 0018-9219(96)01390-4.

I. INTRODUCTION

Currently optical sensor systems, including laser radar, are often limited in performance and cost by mechanical beam directing and stabilization mechanisms. The requisite pointing and stabilization usually requires precise, rapid, mechanical motion, and is often associated with substantial masses. Submicroradian steering precisions are often desired, but are usually impractical for available, affordable, mechanical beam directing systems. Most mechanical systems do not facilitate rapid random pointing. Furthermore, the rapid steering of a large aperture optical sensor often requires a prohibitive amount of power. Despite the considerable accumulated manufacturing experience in this field, mechanical beam steering for optical sensors remains complex, precise, and expensive.

Optical phased arrays appear to have the potential to overcome many of the limitations of mechanical beam steering. Liquid-crystal-based phased arrays require very little prime power, even for large apertures, thereby opening up application areas such as missile interceptors, satellite communications, and portable sensors of all types. Phased arrays are inherently random-access devices, a distinct advantage when regions of interest are distributed widely across a sensor field of regard (FOR). Unlike mechanical systems, liquid crystal devices are generally insensitive to accelerations, and their costs can drop rapidly with volume production, as is the general case for the electronic devices they resemble. Flat panel displays, fabricated using technologies that are similar to those required for liquid-crystal optical phased arrays, are now inexpensive enough to be in every notebook computer.

In the related microwave radar arena, phased arrays are rapidly displacing conventional horn antennas. The clear benefits of random-access, rapid beam pointing with no moving parts have made phased arrays the technology of choice, despite their high cost. Fortunately, cost trades for optical radars using optical phased arrays promise to be more favorable since the optical arrays are monolithically fabricated with no discrete elements, consist of an array of phase shifters rather than individual transmit/receive

modules, and are designed to use low-cost addressing electronics. The optical phased arrays discussed here are passive arrays, consisting soley of phase shifters, and are operated as space-fed arrays, meaning that an already formed beam is fed to the array of phase shifters, which then effects steering of that beam. This contrasts to an active phased array in which individual transmit modules form a beam as it exits a large array of transmitters.

There are many application areas that can benefit from the performance/cost benefits made possible by optical phased arrays. Inexpensive, reliable laser radar for target detection, wind profiling, and gas cloud identification are examples of high interest. Laser communication, whether effected with directed beams in free space or by switching of guided beams within fiber links, is another application area. Defense against infrared guided missiles benefits from directed laser energy, and is another potential optical phased array application area. Later in the paper issues associated with steering broadband optical energy are addressed. Passive infrared sensors for imaging or point detection applications can also benefit from phased array optical beam steering, but to a more limited degree at this time; however, future applications are expected to expand as techniques for reducing the influence of dispersion are developed.

Optical beam steering by means of phased elements is a rich area heavily researched by prior workers. As early as 1971, Meyer [1] had developed a 1-D optical phased array using bulk, lithium tantalate phase shifters. The array comprised 46 phase shifters on one-half millimeter spacings. The number of addressable beam positions, beam widths, scan angles, and beam spacings all were shown to agree with theory as developed for microwave phased array antennas. Shortly thereafter Ninomiya [2] demonstrated a 1-D array of lithium niobate electrooptic prism deflectors. The resolving power of the array was shown to be N times that of a single prism, where N is number of arrayed prisms. The array successfully demonstrated 50 resolvable spots with 600 V applied. Both discrete and continuous steering were demonstrated. The power required was noted to be similar to that for acousto-optic deflectors. Although these early phased arrays clearly demonstrated the concept, they were neither developed for high performance nor were intended for practical application. Large phase shifter spacings of hundreds of wavelengths were unavoidable, given the state of the technology, and precluded achieving efficient large angle beam steering. The small aperture fill factors also guaranteed large insertion losses. However, many of the key advantages of the phased array approach to beam steering were well appreciated by these early workers. Ninomiya pointed out that a phased array offers random access, that the resolving power of a phased array is high, that the steering angle is very accurate, and that there is no shift of optical frequency as with acousto-optic deflectors.

Beam steering of visible light has recently been reported using a liquid crystal television panel as an elementary phased array [3]. Although liquid crystal displays are usually configured to effect intensity modulation, when the polarizers are removed the accompanying phase shift becomes observable. The display pixels are programmed to effect a discrete blazed-grating phase ramp across the aperture. However, the relatively large pixel spacing (several hundred waves), the nonunity array fill factor, and the limited available phase modulation depth (1.3π) have severely limited the achievable steering efficiency and angle ($<0.1°$).

Other workers in the field have attempted to develop higher performance optical phased arrays by greatly reducing the phase shifter spacings. Vasey *et al.* [4] have developed an integrated optics approach comprising a 1-D phased array based on a linear array of closely spaced AlGaAs waveguides, the relative phases of which can be electrically adjusted using the electrooptic effect in the waveguiding material itself. Beams are coupled into the guided structure and launched into free space using grating couplers. Continuous steering is achieved by electrically imposing a linear phase ramp of adjustable slope across the aperture. Addressing is accomplished via a fine/coarse architecture, somewhat similar to the approach discussed in Section IV. Continuous steering of a 900 nm beam over a ± 7.5 mrad field has been reported. Element spacings are orders of magnitude less than those in earlier bulk demonstrations, but remain multiple (13–14) wavelengths. Consequently, maximum steering angles are limited and efficiencies are low due to the large number of radiated diffraction orders (so-called grating lobes). Although the electrooptic effect used in this approach is inherently fast (ns), achieving the steering angles and efficiency levels required for laser radar is expected to be difficult, as is scaling to required aperture sizes and obtaining steering in two-dimensions.

Another approach reported recently [5] uses a thin, 2-D array of liquid crystal phase shifting elements configured to operate as coherent microprisms with a relatively high fill factor. The individual elements are multiple wavelengths in extent and spacing, but are constructed to produce a linear phase ramp of adjustable slope across each element face, thereby simulating a discrete blazed grating with programmable blaze angle. The current device steers in one dimension only, although in principal two devices could be cascaded to steer in both dimensions. Unlike most preceding optical arrays, this device was specifically designed for laser radar application and is, in principle, capable of high efficiency at large angles (20°) and of being fabricated with large apertures. However, to date, only small apertures (2 mm square), moderate steering angles (5°), and low efficiencies (1%–9%) have been achieved owing to fabrication difficulties inherent to the approach. One of the difficulties is that this approach requires using only the linear portion of the liquid crystal versus voltage curve, resulting in a limited use of available birefringence.

A more classic approach to optical phased arrays has been under development by the authors. This work has resulted in development of a true optical phased array with 1-D phase shifter spacings smaller than a single free-space wavelength, 100% aperture fill factors over significant apertures, and performance approaching theoretical predictions for small to moderate angles. The unity fill factor, small phase

shifter spacings, and careful fabrication techniques used result in very low sidelobe levels. These are the first optical phased arrays which are capable of redirecting a single input beam into essentially a single, diffraction limited, output beam with negligible sidelobes. Using this approach, high performance optical phased array based steering of carbon dioxide laser beams (10.6 μm) was first demonstrated in 1989, with demonstrations of Nd:YAG steering (1.06 μm) following soon thereafter [6], [7]. That work will soon appear in the open, reviewed, literature [8], [9].

These new optical phased arrays are direct functional analogs of the well known microwave phased array antennas [10] that make possible the agile, inertialess steering of microwave beams. The underlying fundamental concepts are identical to those for a microwave array. However, due to the orders-of-magnitude difference in wavelengths between the microwave and optical worlds, these new optical phased arrays have been implemented quite differently. The current optical devices are 1-D, space-fed, passive, phase-only, apertures. This differs from modern microwave phased arrays with which a beam is usually both formed and steered in two dimensions by a 2-D array of active elements. The field intensity across the aperture of an active microwave array is generally tapered at the edges in order to achieve low sidelobe levels. This is not an option with a passive, phase-only array. However, being space-fed, if the input optical beam is Gaussian in spatial profile, as is the usual case, additional tapering is not needed. The 1-D phase-only array steers an optical beam in one dimension only. Unlike modern microwave arrays, and most other optical phased arrays to date, these new arrays are designed to be easily cascaded. This allows simple mounting of orthogonal 1-D arrays to steer the beam in two dimensions. Microwave arrays are built using discrete phase shifters, as have been most early optical phased arrays. However, since a vast number of phase shifters is needed to realize a high performance optical array, distributed liquid crystal phase shifters have been implemented, as described by Huignard *et al.* [11]; however, it has proven essential to implement additional innovative addressing means to avoid the otherwise impractical numbers of interconnects.

The organization of this paper is as follows. In Section II liquid crystal optical phased array technology is summarized. In Section III we briefly discuss alternative candidates to optical phased arrays for eliminating complex and expensive mechanical motion from laser radar optical systems. A more detailed description is presented in section IV. Section V summarizes performance levels achieved and predicted performance potential. Section VI considers the pointing of an acquisition sensor, often a passive infrared (IR) sensor. Section VII discusses laser radar system concepts that incorporate target acquisition and tracking capabilities. Section VIII contains conclusions.

II. Overview of Liquid Crystal Optical Phased Array Concepts

A prism inserted into the aperture of an optical system introduces a linear gradient of optical path delay (OPD) across the aperture which tilts the phase front and thereby steers the optical beam. For a given wavelength a phase shift of 2π (corresponding to an OPD of one wavelength) can be subtracted periodically from the phase front without influencing the far-field pattern produced by the phase front [12]. The "folded" phase profile represents a blazed grating. The phase ramp, or its equivalent modulo-2π sawtooth phase profile, further can be approximated by a series of discrete phase steps, as long as the steps are small.

Fig. 1 illustrates the use of nematic liquid crystal cells as phase shifters. With no applied fields, the liquid crystal molecules align with an average orientation parallel to the substrates, according to the liquid crystal alignment layer applied at the substrate interface. Application of a relatively low voltage, on the order of 1–10 V, reorients the liquid crystal molecules and changes the effective index of refraction as seen by light polarized along the direction of quiescent molecular orientation. The maximum phase shift available is proportional to the thickness of the liquid crystal layer. The case of a 2π phase retarder is illustrated. The switching speed of a nematic liquid crystal phase shifter is generally inversely proportional to the square of the thickness of the nematic liquid crystal layer [13]. For steering angle/aperture size combinations that require phase resets, the minimum thickness of the liquid crystal layer to produce efficient steering requires a liquid crystal layer sufficiently thick to produce a full wavelength of OPD and allow modulo 2π operation. Only a combination of very small angles, or very small aperture size, allows practical beam steering without the use of resets. The liquid crystal layer thickness, t, for a 2π phase shift is given by

$$t \geq \lambda/\Delta n \tag{1}$$

where $\Delta n = (n_e - n_o)$ is the birefringence of the material and λ is the free space wavelength. As an example, the nematic liquid crystal E7 has a birefringence of approximately 0.2 in the visible and near infrared spectrum. It requires a 5 μm layer thickness to achieve a relative phase delay of 2π radians at a 1 μm wavelength. If a reflective-mode design is used, allowing two passes through the liquid crystal layer, a full wave OPD is created using only half that thickness, or 2.5 μm.

The diffraction efficiency, η, of a grating with a stair-step blaze designed to maximize energy in the first order is given by [23]:

$$\eta = \left(\frac{\sin(\pi/q)}{\pi/q}\right)^2 \tag{2}$$

where q is the number of steps in the blaze profile. From (2) it can be seen that an eight-step approximation gives a theoretical efficiency of approximately 95%. Fig. 2 shows a step approximation to the wavefront deflected by a prism, including the 2π phase resets. Note that a 2π phase reset has that value only for the design wavelength. Fig. 3 shows the deviation from a straight line in the unfolded phase profile when a wavelength other than the design wavelength is used. This variation in phase reset values causes dispersion

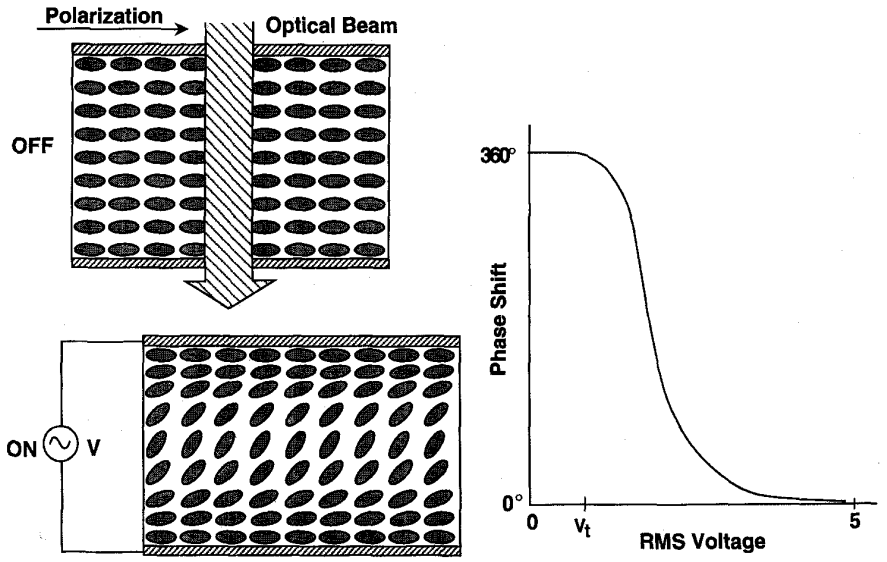

Fig. 1. Nematic liquid crystal phase shifters. The liquid crystal molecules are birefringent. Light polarized along the long axis of the molecule will experience a different index of refraction than light polarized along the short axis of the crystal. The molecules will rotate when a voltage is applied, producing an effective index change for light polarized perpendicular to the long axis of the crystal.

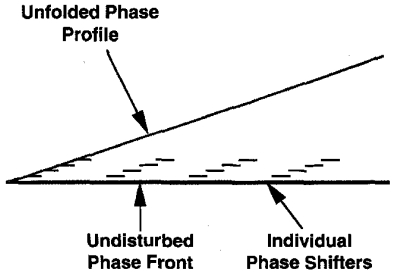

Fig. 2. *Optical phased array agile beam steering.* The optical phase delay introduced by a prism in an aperture can be approximated by a series of stair-step ramp phase delays. When a ramp has an optical path difference equal to or larger than the design wavelength one design wavelength of optical path difference is subtracted from the ramp. At the design wavelength, the phased array effectively reproduces the steering caused by a prism.

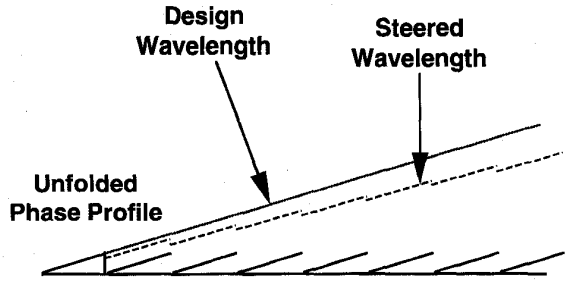

Fig. 3. *Unfolded phase profile.* This figure shows the influence on the unfolded phase profile of operation at a wavelength other than the design wavelength.

[14], which will be discussed further in Section VI. As shown in Fig. 3, the unfolded OPD is in error by $(\lambda - \lambda_d)$ after each reset, and the unfolded phase is in error by $2\pi(\lambda - \lambda_d)/\lambda$ after each reset, where λ is the actual wavelength and λ_d is the design wavelength.

Practical factors can cause the measured efficiency of an actual phased array beam steerer to deviate from the theoretical value given by (2). One such factor, evident in liquid crystal phased arrays currently being developed, is a spatial "flyback" in the molecular orientation of the liquid crystals which results from the minimum spatial extent required to change from the orientation for a phase shift of 2π to that for a phase shift of zero. The actual flyback transition is a complex function of device design and liquid crystal visco-mechanical properties. Fig. 4 depicts phase versus position for a simple flyback model. As a result of flyback, only a portion of the grating imposes the correct phase distribution to steer a beam in the design direction. That portion of the grating over which flyback occurs can be thought of as steering the beam in a different direction. The resulting diffraction efficiency η into the desired grating order can be approximated by [15]

$$\eta = \left(1 - \frac{\Lambda_F}{\Lambda}\right)^2 \tag{3}$$

where Λ_F is the width of the flyback region and Λ is the period of the programmed grating. The energy that is not directed into the desired grating order is distributed among numerous other grating orders, causing a loss in efficiency for the primary order. The overall steering efficiency is given by the product of (2) and (3). Depending on the grating period (which affects both the number of steps in the blaze profile as well as the relative size of the flyback),

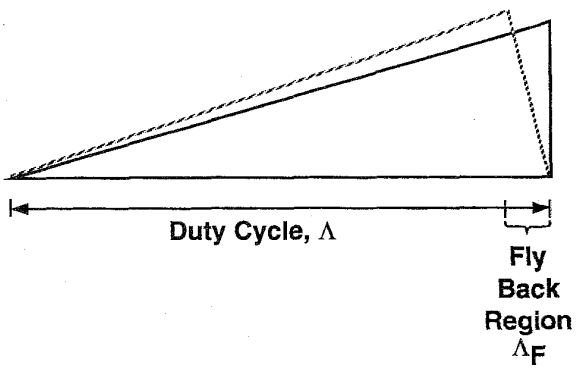

Fig. 4. *Flyback.* When one design wavelength of optical path difference is subtracted it requires finite spatial extent. This region is referred to as the flyback region. The steering efficiency into a given order is influenced by the relative size of the flyback region with respect to the grating period.

either (2) or (3) may dominate the overall steering efficiency of an optical phased array beam steerer.

For a normally incident input beam the steered angle is given by [16]

$$\sin\theta = \frac{\lambda_o}{\Lambda} \tag{4}$$

where λ_o is the design wavelength for the beam steerer, $\Lambda = qd$ is the period of the staircase ramp, q is the number of phase shifters between resets, and d is the center-to-center spacing between phase shifters, which is assumed to equal the width of the phase shifter as well. Large steering angles correspond to high spatial frequencies (small periods) and vice versa. From (3) and (4) it can be seen that the steering efficiency decreases monotonically with steering angle, for fixed flyback.

Two-dimensional beam steering can be achieved using two orthogonally oriented 1-D liquid crystal phase gratings. In addition, any optical distortion that is separable in Cartesian coordinates can be fully compensated, modulo 2π. Spherical aberrations can be fully compensated with a crossed grating system. For a full adaptive optics capability, a third layer, with a 2-D array of phase shifters, would be required. This would add the ability to clean up an arbitrarily aberrated beam and adapt for atmospheric turbulence. Such a liquid crystal adaptive optics layer has recently been discussed [17]. The spacing of elements on such an adaptive optics layer would be orders of magnitude courser than the spacing required for large angle beam steering. Current adaptive optics mirror systems have on the order of 50–400 elements correcting for turbulence while using apertures up to a few meters [18]. However, the adaptive optic element is usually used prior to final beam expansion and is much smaller in aperture. Pixelated phase shifters of about 1 mm square would probably suffice for most applications and could be readily fabricated with the current technology. Thus liquid crystal phase shifter technology could replace the current piezoelectrically driven adaptive optic components, resulting in a single three-layer component that both deflects and phase compensates a beam. If operated modulo 2π, such adaptive optic elements would be dispersion limited to narrow band applications.

III. Beam Steering Approaches Using Limited Mechanical Motion

An optical phased array is not the only approach to realizing rapid beam steering without the use of conventional mechanical systems. Some of the more viable alternate options are briefly reviewed here. All of the options discussed here potentially allow the redirection of the field-of-view of an optical sensor without the use of complex, costly, mechanical mechanisms. Unlike the optical phased array, most of these alternate options do not eliminate mechanical motion, but instead minimize the degree of mechanical motion required. To date, none of these alternate approaches have demonstrated the scope of performance characteristics desired for laser radar and most other optical sensors.

One such option is the use of cascaded microlens arrays [19], [20] an example of which is shown in Fig. 5. Each microlens array consists of a (generally) close packed, periodic array of miniature lenses which can be fabricated in either diffractive or refractive forms. Beam steering is effected by translating one microlens array with respect to the other. The concept can be understood by first considering a single microlens pair from a set of aligned afocal arrays. A collimated input beam is focused to the back focal point of the first microlens, which is also the front focal point of the second microlens, resulting in an unsteered, collimated output beam. However, if the second microlens is offset, then the back focal point of the first microlens appears as an off-axis point to the second microlens. The point remains in the front focal plane of the second microlens, so the second microlens still recollimates the light, but the beam is redirected to a nonzero field angle. A paraxial ray trace shows that the tangent of this field angle is equal to the amount of offset divided by the focal length of the second microlens. Maximum useful steering occurs with an offset equal to the radius of a microlens. It may be noted that it does not matter if the second microlens has a positive or negative focal length so long as the condition of overlapping focal planes is met. If the individual microlenses of the arrays are aligned, periodically spaced, and designed to fill the aperture, the output beam replicates the input beam. If the offset is small, the steered beam approximates a simple redirection of the input beam.

However, if the offset is large, significant fractions of the input beam are coupled into other grating modes. This can be appreciated by noting that phased arrays and microlens arrays both approximate blazed gratings [21]. If the periodic quadratic phase profiles of two offset microlens arrays are superimposed, the result is a (generally asymmetric) triangular waveform, which approximates a blazed grating. If the composite phase profile were a sawtooth, the approximation would be exact. Motion of the lenses alters the slope(s) of the phase profile, thereby changing the blaze

profile of the equivalent grating, and shifting the light to different grating orders. To the extent that the composite phase profile approximates a true sawtooth, light is steered to a single direction. However, the offset of two lens arrays inherently causes each input lenslet to illuminate adjacent output lenslets, resulting in the multiple-slope profile of the triangular wave, and steering to multiple directions. To mitigate this effect, designs using a third microlens array as a field lens have been put forth, but demonstrations have not yet been reported.

The agile steering of a beam using the microlens array concept requires the agile motion of one microlens array with respect to the other. Microlens arrays inherently have small focal lengths (typically on the order of a few lenslet diameters, usually a millimeter or less); consequently, the amount of mechanical offset required to achieve a desired steering angle can also be quite small. Compared to steering via a displaced bulk lens having the same aperture as the microlens array, the reduction of motion required to steer to a given angle is proportional to the ratio of the individual microlens diameter to the array diameter. Due to its essentially planar structure, a microlens array can be made much lighter than a bulk lens of equivalent aperture. The combination of low mass and small motion allows agile positioning (and agile beam steering) to be accomplished with more simplified mechanical drivers than would be required for macroscopic lenses. The microlens arrays can be designed to effect substantial steering with mechanical motions that can be achieved with piezoelectric transducers. However, small errors in mechanical positioning are amplified by the same optical leverage that makes possible the reduction in mechanical motion. This means the amount of energy at the desired steering angle will be influenced by a small amount of mechanical motion. Thus fine angular beam steering with this approach generally requires very precise motion.

Microlens arrays can be programmed onto the liquid-crystal based optical phased arrays reported here, thereby making possible an electronic translation of one lens array with respect to the other, and complete elimination of all mechanical motion. Since only one microlens array must move to achieve beam steering, only a single array would have to be programmable. Owing to the precise displacement control available with an optical phased array, this option may be preferable to piezoelectrically driven motion for applications requiring precision pointing.

Flexure beam micromirror technology is another approach with large numbers of small apertures arranged in regular arrays [22]. The individual apertures are lithographically fabricated mirror "pixels" on hinges with micromotion effected by an electrostatic field. The field attracts the element and moves it rapidly, on the order of a microsecond. This can create a piston phase shift for the individual aperture. These devices have demonstrated 2π phase shifts at 633 nm wavelength with a 60–75% fill factor. Much of the same phased array theory discussed later in this paper applies to these array structures, although the physical implementation is significantly different. The implementation

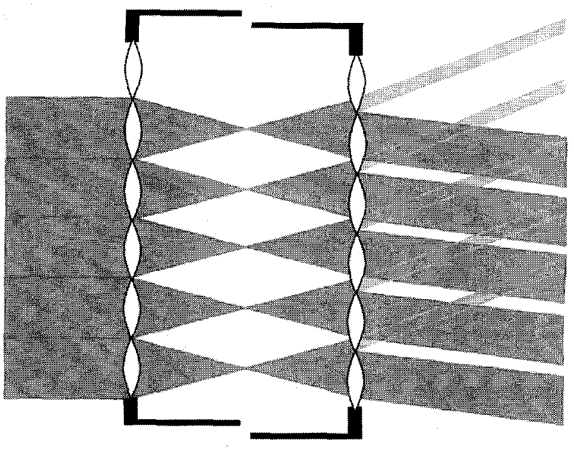

Fig. 5. *Decentered microlens array beam steering.* The figure shows two decentered microlens arrays, and their influence in steering an incoming beam. If one array is moved with respect to the other array it causes the beam to steer.

of this approach makes individual apertures with sizes on the order of visible or near infrared wavelengths impractical, thus limiting maximum steering angles. A second limitation is the nonunity fill factor. Hidden hinge concepts are being considered to address the fill factor issue [23].

Different approaches are represented by electro-optical (EO) and acoustic-optical (AO) beam deflection [24]. There are no moving parts with either approach. EO deflection can occur in nanoseconds, while AO beam deflection is generally effected on the order of microseconds, the time for an acoustic wave to propagate across the crystal aperture. AO beam steering requires high drive power at longer wavelengths, has an aperture size limited by available crystal dimensions, and shifts the frequency of the transmitted, or receive, beam. EO beam deflectors require high voltages for large apertures, typically of the order of 10 kV/cm. Beam deflection angles for both EO and AO deflectors are typically limited by practical issues to a few milliradians; consequently, these devices are generally restricted in applications to fast, fine beam steering of small beams. Optical beam deflectors based on electrooptic and acousto-optic effects have been widely reviewed [25]–[28] elsewhere. Such devices are not generally configured as phased arrays.

Agile optical beam steering with limited mechanical motion can also be effected using the Roving Fovea concept [29]. Fig. 6 shows a schematic representation of a roving fovea beam director. With this approach a light weight "pistol" support for the secondary mirror of a telescope is moved substantially, but due to the relatively low mass, the operation steering can be accomplished rapidly. The "pistol" is made to rotate about the center of curvature of the primary mirror of a Cassegrainian telescope. It has a length equal to one-half the distance between the mirror and the center of curvature. Light exits the secondary optical element mounted on the "pistol" at the focal length of the mirror. The beam diverges to a size less than the mirror diameter. This beam size establishes the effective

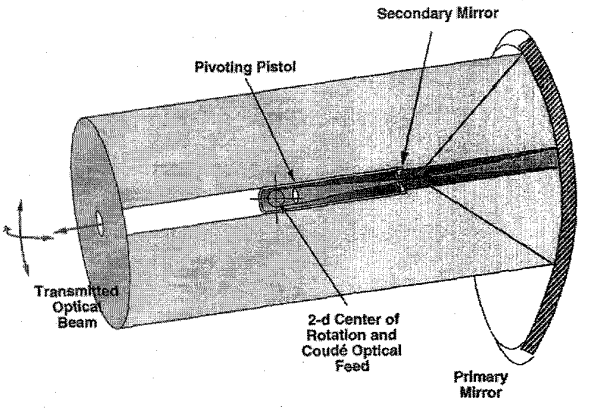

Fig. 6. *Roving Fovea agile beam steerer.* The pistol rotates around the center of curvature, thus steering the collimated optical beam while moving only a small mass.

steered aperture. The primary mirror collimates the light and reflects it along the axis of the pistol. As the pistol rotates about the center of curvature, so does the optical field of view, and the direction of the collimated beam changes. The primary mirror needs to be oversized to accommodate the extended range of motion of the beam on the primary mirror. Larger angular deflection requires a larger primary mirror. The effective beam size is shown by the area labeled "transmitted optical beam."

IV. Optical Phased Array Concepts and Architectures

Optical phased arrays are direct functional analogs of the well known microwave phased array antennas [10] that make possible agile, inertialess steering of microwave beams. Fig. 7 illustrates the use of a 1-D, space-fed, passive, phase-only, optical phased array to steer the output beam of a laser radar by electrical control of the array of phase shifters on the system output aperture. This differs from many modern microwave phased arrays in which the beam itself is formed at a 2-D array by active elements, and steered by that array in two dimensions. Here the laser beam is already formed. It is Gaussian in spatial profile. It is not necessary to electrically program the beam amplitude across the output aperture to achieve low sidelobe levels. The 1-D phase-only array steers the laser beam in one dimension. It is interesting to note that recent attention to more affordable microwave phased array architectures has brought the space fed configuration to a more prominent position in microwave phased arrays [30].

A. One-Dimensional Phased Arrays

The concepts underlying operation of an optical phased array are identical to those for microwave arrays. Orders-of-magnitude differences in wavelength between the microwave and optical worlds has resulted in a different implementation of practical optical phased arrays than that taken with microwave arrays. Innovative design features used to bring the fabrication and operational requirements

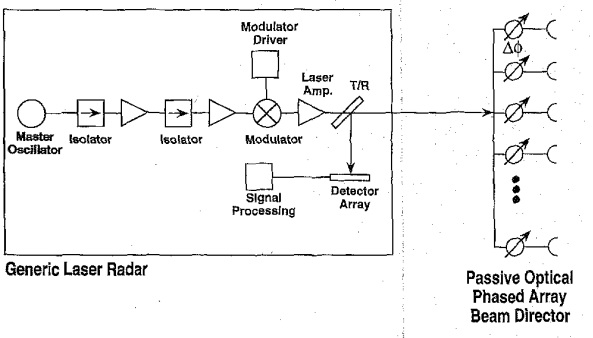

Fig. 7. *Block diagram of a laser radar using a space fed phased array.* The beam is already formed, then passes through an array of phase shifters.

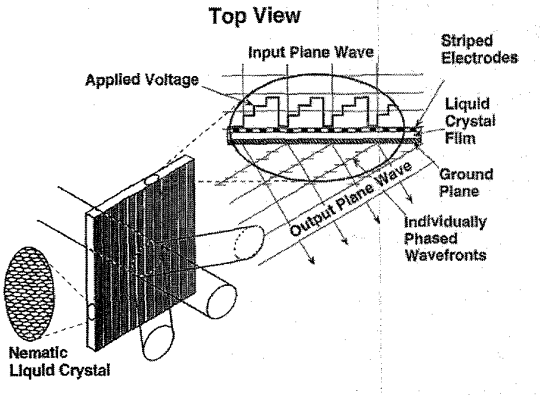

Fig. 8. View of a 1-D beam steerer, and a conceptual imposed phase shift.

of an optical phased array within the reach of currently available, practical technology are discussed, as are some specific architectures in current use.

Fig. 8 illustrates a transmission mode optical phased array beam steerer comprised of a 1-D array of equi-spaced liquid crystal phase shifters. The inner surface of one transparent substrate is photo-lithographically patterned with transparent, conducting, striped electrodes having the desired spacing for the phase shifters in the array. The entire active aperture of the array is so patterned. The inside of the other substrate is coated with a uniform, transparent, conducting ground plane. Both substrates have inner surfaces prepared to effect quiescent liquid crystal alignment. Application of a voltage between any given striped electrode and the underlying ground plane creates a 1-D phase shifter in the liquid crystal volume underlying the patterned electrode. The liquid crystal film is continuous; i.e., there are no specific hard boundaries inserted between the individual phase shifters. Thus a multitude of optical phase shifters is formed by simply assembling the two cell substrates with the proper spacing. This is a key aspect of the optical phased array design approach and a point of significant design deviation from microwave phased arrays, where phase shifters are discrete rather than distributed.

Application of a periodic sequence of staircase voltage ramps of period L across the array aperture creates a

corresponding periodic staircase profile of phase, as shown in the expanded portion of Fig. 8. With properly weighted voltage steps, chosen to compensate for the nonlinear phase-voltage profile of a typical liquid crystal, a linearly increasing phase profile can be produced. If the maximal phase shift on each staircase ramp of q voltage steps is $2\pi(q-1)/q$, the periodic (modulo 2π) phase profile is equivalent to a single staircase phase ramp across the aperture. An electronically adjustable prism is simulated, and the beam is steered to a new direction θ (relative to the phased array boresite) given by the general grating equation,

$$\sin\theta + \sin\theta_{\text{inc}} = \frac{\lambda_0}{\Lambda} \tag{5}$$

where θ_{inc} is the incident angle of the beam, and the other parameters are the same as in (3). The steering direction depends on the periodicity (and sign) of the applied voltage ramp. The device operates in identical fashion for both transmit and receive modes.

Fabrication of an optical phased array can be quite similar to that of a liquid crystal display. Cross sectional and perspective views of a typical optical phased array are shown in Fig. 9, illustrating the key features. Electrical contacts to the transparent, thin-film electrode pattern can be made on the periphery of the aperture using deposited metal leadouts, not shown in the figure. The perspective view illustrates the option of on-array addressing circuitry. An insulating, antireflection coating is applied over a lithographically formed electrode pattern, followed by a thin-film liquid crystal alignment layer. The alignment layer is chosen to provide a fixed, finite tilt bias of the boundary layer liquid crystal molecules in order to minimize undesirable domain formations as voltages are applied to the electrodes. A second substrate is fabricated with a uniform conductive, transparent thin-film ground plane, followed by antireflective and liquid crystal alignment layers. The external surfaces of both substrates are also provided with antireflection layers.

The two substrates are brought together with uniform spacing using, for example, precision glass rod spacers. The substrates are secured with adhesive applied over the perimeter of the active region, with exception of a small liquid crystal fill hole. The volume between the substrates is then vacuum filled with liquid crystal. For much of the work reported here, the E7 liquid crystal mixture manufactured by BDH was used. Silicon addressing chips are typically mounted to the overlapping surface of the electrode containing substrate and wirebonded to leadout metallization pads. The inputs to the chips are then wirebonded to a supporting frame, on which is mounted an electrical connector leading to the control computer.

Reflective-mode analogs are straightforward and have been demonstrated. The transparent ground plane can be replaced by either a metal mirror or a dielectric mirror with a transparent, conducting overlayer. An advantage of the reflective-mode design is switching speed. The double-pass path through the liquid crystal allows operation with

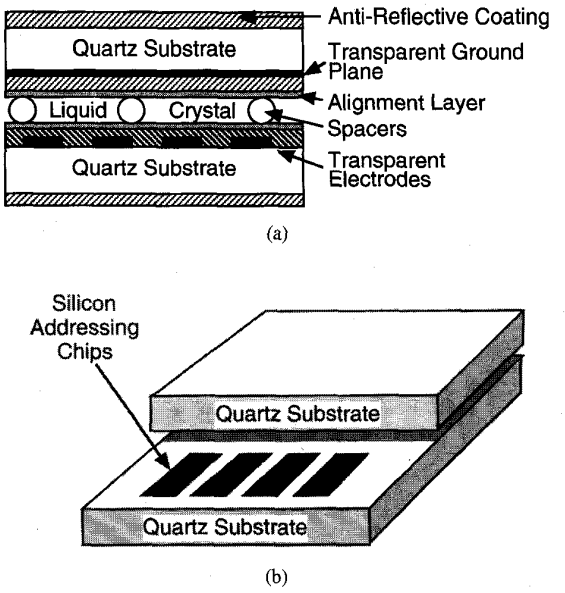

Fig. 9. Liquid crystal device cross section and perspective views.

one-half the thickness of the transmission-mode case. This results in four times the switching speed, as discussed in Section IV-C. An additional potential advantage is the superior heat sinking afforded with a face-cooled rather than an edge cooled geometry.

The above description considers the 1-D phased array as an electrically tunable blazed grating. An alternate description follows from the analogy to a 1-D microwave phased array, for which numerous analyses are available. The following expressions follow from Skolnik [10]. The normalized intensity radiation pattern, I, for a 1-D array of phase shifters can be written compactly as

$$I = [\sin^2(N\alpha)/\sin^2(\alpha)]/N^2 \tag{6}$$

with

$$\alpha = \pi(d/\lambda)(\sin\theta - \sin\psi) \tag{7}$$

and

$$\sin\psi \equiv \lambda\phi/(2\pi d) \tag{8}$$

where θ is the angle (relative to array boresight) at which the field is measured, N is the number of phase shifters in the array, d the (uniform) spacing of the phase shifters which are assumed to have uniform phase difference ϕ between elements, and λ is the free-space wavelength. Each phase shifter has a far-field pattern of its own, in accordance with its width. The interference among the individual antenna patterns from all the phase shifters in the array creates the narrow antenna pattern (6) which has an intensity maximum at angle ψ; i.e., $\psi(\phi)$ is the angle to which the beam is steered. Note that the steering direction given by (8) is equivalent to that of (5) with $\Lambda = 2\pi d/\varphi$, which is just the distance across the array needed to accumulate a phase difference of one wave.

The optical phased array far-field beamwidth, θ_B, follows from (6) and (7) and is approximately given by:

$$\theta_B = a\lambda/(Nd\cos\psi). \tag{9}$$

Here a is a near-unity constant which depends on the shape of the array, the illumination profile, and the definition of beamwidth as full-width or half-width at half-max or $1/e$ levels. For uniform illumination of a square aperture with a full beamwidth at half-max intensity definition, $a = 0.886$. For a circular aperture with uniform illumination and half-beamwidth measured at the first Airy null, $a = 1.22$. The dependence of beamwidth on steering angle is negligible for the 0–10° range, and a reasonable rule of thumb for beamwidth is just $\theta_B = \lambda/D$, where D is the aperture diameter, $D = Nd$. Optical beam widths are vary narrow by microwave standards. Typical microwave radars have beamwidths measured in degrees or milliradians, whereas typical optical apertures yield beamwidths measured in microradians. A 10 GHz phased array with a beamwidth similar to that of a 10 cm optical aperture at 1 μm would have to be approximately 3 km in diameter.

Fig. 10 illustrates in greater detail the desired phase profiles for a beam steerer and a corresponding far-field pattern, calculated by Fourier transforming the near-field (aperture) phase profile. The aperture scale corresponds to operation at 1.06 μm. The ideal beam steering phase front is the linear phase ramp, which simulates the optical path delay (OPD) of a prism, redirecting the beam direction according to the slope of the phase front. The ideal linear phase ramp gives just one beam out for one beam in and generates no sidelobes. To maintain speed of response it is necessary to restrict the magnitudes of the phase shifts to the order of a single wave, as discussed earlier. For a given wavelength a phase factor of 2π, corresponding to an OPD of one wavelength, can be periodically subtracted from the phase profile without influencing the far-field pattern. The ideal practical ramp becomes the modulo-2π sawtooth ramp shown. The 2π sawtooth ramp also steers with unity efficiency (no sidelobes), but only for the particular wavelength for which the phase resets are exactly 2π radians. This variation in reset phase value with wavelength causes dispersion.

It is usually convenient to digitize the voltage input, resulting in a staircase-like (digitized) phase ramp, illustrated here for the case of 3-b (8-state) equispaced quantization. The intensity diffraction efficiency, η, of a grating with a stair-step blaze designed to optimize energy in the first order is given by (1). The 3-b quantization case shown gives a theoretical efficiency of approximately 95%. The 5% energy "loss" is coupled into the various sidelobes or higher-order diffraction orders, the largest for this case being schematically depicted at about 250 mrad. Finer quantization gives higher efficiency and correspondingly lower sidelobe levels. Actual devices can show somewhat higher efficiencies at small angles due to roundoff of the quantized stair-step edges as a result of finite spatial response of the liquid crystals as described below.

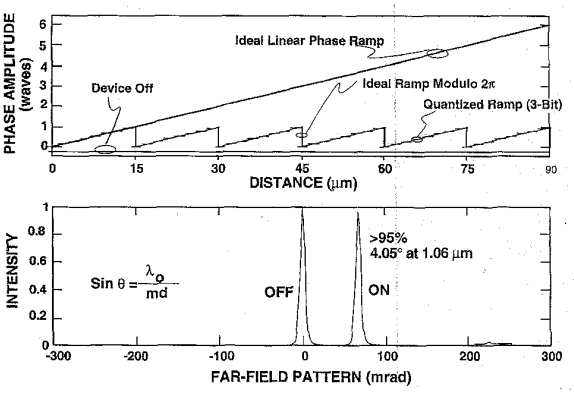

Fig. 10. Optical Phased Array Phase Profile and Steered Beam Antenna Pattern (4° beam steering is shown, based upon an imposed phase shift profile).

The ideal sawtooth phase profile cannot be realized exactly. Fringing electric fields and the viscosity of liquid crystals cause the phase resets to occur over a finite spatial extent. Equation (4) gives the first order efficiency resulting from flyback. The flyback period can be modeled electrostatically, accounting for the nonlinear behavior of the liquid crystal. The flyback distance is typically approximately equal to the liquid crystal cell thickness. Depending on the steering angle (the grating period affects both the number of steps in the phase profile as well as the relative size of the flyback), either prism quantization or flyback efficiencies may dominate the overall steering efficiency.

The above discussions point out that the steering *efficiency* depends on the shape of the phase profile. The steering *direction*, however, is independent of the ramp details; it depends only on wavelength, grating period (which is lithographically determined to parts per million accuracy), and incident angle, according to the grating equation.

Additional sidelobes can arise from over-illumination of the array aperture. For a circular aperture the sidelobes form an Airy pattern of continuous rings, whereas the grating sidelobes discussed above are essentially delta functions in angle space. The peak intensity of the first sidelobe for uniform illumination of a circular array aperture is approximately 13.3 dB below the peak intensity of the main beam. For illumination by a Gaussian beam truncated at $1/e$, it is approximately 20.9 dB below the main beam; the sidelobes decrease uniformly with less beam truncation. These sidelobe characteristics are identical to those of microwave phased arrays; the sidelobe values follow from expressions for circular apertures.

Fig. 11 illustrates the motivation for choosing a 1-D phased array architecture. Typical phased arrays (almost all microwave arrays) use a phase shifter spacing of approximately one-half wavelength to avoid the undesirable generation of higher-order grating modes. Assuming such spacing, the number of array elements (phase shifters) required to fill a given $D \times D$ square aperture is plotted. A number of well known microwave arrays are approximately located in this parameter space by their names. The data are

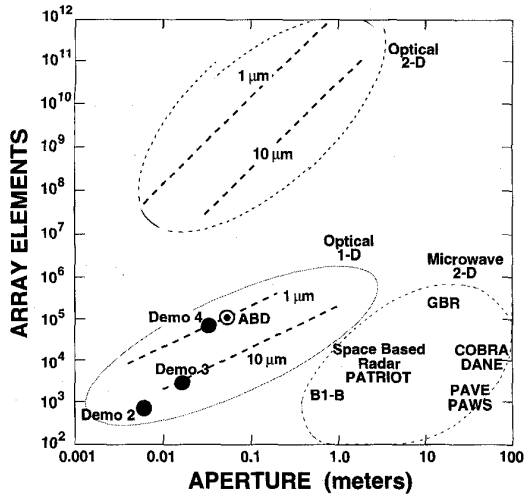

Fig. 11. *Addressing requirements for various phased array configurations.* This graph shows the advantage in terms of required number of addressing leads between 1-D arrays instead of 2-D arrays.

taken from Brookner [31]. If an optical phased array were constructed in the same manner as the classic microwave arrays, with a 2-D phase shifter pixelation, the curves labeled "optical 2-D" would be obtained. The number of phase shifters needed grows as $(2D/\lambda)^2$. Assuming a minimum of one control lead per phase shifter, it is seen that on the order of one trillion leadouts would be required for optical 2-D phased arrays of desirable apertures. Far-infrared arrays would require "only" billions of leads. Such numbers are far beyond the capabilities of any known leadout technology. For a basis of comparison, consider a megapixel active matrix display, which probably represents the current state of the art for leadout quantity and is realized only by using highly multiplexed addressing schemes. A megapixel 2-D optical phased array with $\lambda/2$ pixel spacing would only subtend a one-half millimeter square aperture for 1.0 μm light, and therefore would be far too small for many of the sensor applications of interest. One-dimensional arrays, however, grow only as $2D/\lambda$, and have correspondingly reduced leadout requirements, as shown. Designs for various demonstration devices already developed and demonstrated are depicted by solid circles; a next-generation array under development is indicated by the open circle, labeled ABD.

B. 2-D Steering

Two-dimensional steering is readily accomplished by cascading two 1-D steering arrays with crossed electrode patterns: one for azimuth (AZ), and one for elevation (EL). The cascading can use individual, discrete, steering devices. Relay lenses can be used to avoid beam walkoff between the devices, as is sometimes done with mechanical steerers [32]. However, the inherently thin format of these liquid crystal cells has to date obviated the need for such relay lenses. The availability of both reflection- and transmission-mode variants facilitates the design of cascaded systems. An attractive prospect is the integration of AZ and EL steering units into a single, thin cell, potentially conformal with an airframe. Current optical phased array designs are polarization dependent; they require the input beam to be linearly polarized along the direction of quiescent liquid crystal alignment for maximal efficiency. Orthogonally polarized incident energy experiences no phase shift between the "on" and "off" states, and is not steered. Consequently, if the cascaded 1-D arrays are identical, a 90° polarization rotator (such as a half-wave plate) must be inserted between the arrays. Alternatively, the arrays can be constructed with orthogonal sensitivity axes, thereby eliminating the need for polarization rotation. This approach is preferred for larger aperture devices, due to the general unavailability of large aperture polarization components, particularly at the longer wavelengths. Both approaches have been successfully demonstrated. By doubling the number of steering layers it is possible to steer both polarizations.

C. Liquid Crystal Phase Shifters

Nematic-phase liquid crystals offer a number of unique characteristics that, for the first time, make possible the practical implementation of high-performance optical phased arrays. Fig. 9 illustrates a typical liquid crystal cell formed from two transparent substrates and a thin layer of liquid crystal (1–50 μm depending on the wavelength and material). The substrates are prepared with an alignment layer that gives a preferential initial alignment to the molecules adjacent a substrate surface. Cooperative forces among the liquid crystal molecules then align the entire cell volume, as illustrated for the "off" condition. Under this condition an input optical beam polarized parallel to the long axis of the liquid crystal molecules samples the extraordinary index of refraction, n_e, of the (birefringent) liquid crystal. When a voltage exceeding the threshold voltage V_t is applied across the liquid crystal film, the molecules tend to align with the field, thereby altering the apparent index, to a limit that asymptotically reaches the ordinary index, n_o. With proper choice of cell thickness, t, the differential phase shift $\Delta\phi$ between "off" and "on" conditions,

$$\Delta\phi = \frac{2\pi(n_e - n_0)t}{\lambda} \tag{10}$$

can be set to exactly one wave, or 2π. Here λ is again the free-space wavelength. The liquid crystal birefringence, $\Delta = (n_e - n_o)$, is typically [33] in the range of 0.05 to 0.3. The molecular orientation, and the phase shift, is responsive to the rms. value of the applied voltage, which is typically a 1–10 kHz sinusoid in the 1–10 V range. The reverse s-shaped response shown is typical of nematic liquid crystals. The waveform of the electrical driving signal can be chosen to be a square wave if frequency sidelobes are to be avoided.

Much of the optical phased array development to date has been based on the nematic material E7, which has a birefringence of about 0.2 in the infrared. This means that

a transmission cell need be only five waves thick to induce a full wave of differential phase shift. The birefringence of liquid crystals greatly exceeds that available with most other known materials. For comparison, lithium tantalate, one of the best conventional bulk electro-optic materials, has a birefringence of only 0.00015 (at 10 000 V/cm). Propagation through about 7000 waves would be required for a full-wave phase shift at 1.06 μm wavelength. Furthermore, the high voltages required would be quite incompatible with the high-density integrated circuitry needed to address and drive practical optical phased arrays. The relatively thick layers required also would lead to poor spatial resolution on the phased array due to fringing of electrical addressing fields, thereby limiting steering to relatively small angles. Further advantages of liquid crystals include a very low power density required for addressing, typically a few $\mu W/cm^2$ for displays of similar construction [34], and the ability to fabricate phase shifters lithographically to dimensions of the order of a wavelength.

The dynamics of liquid crystal director motion may be modeled in a parallel-aligned geometry using the Leslie–Ericksen equation [34]. Using several simplifying assumptions it may be shown that the liquid crystal director relaxes back to its equilibrium configuration following an exponential decay with time constant

$$\tau_d = t^2\gamma/(k\pi^2) \tag{11}$$

where t is the cell thickness, γ the effective viscosity, and κ the effective elastic constant. The turn-on (rise) time is field driven and given by

$$\tau_r = \tau_d/[(V/V_t)^2 - 1] \tag{12}$$

where V is the applied voltage and V_t the threshold voltage. Under normal operating conditions, with $V > \sqrt{2}V_t$, the decay time (11) limits the switching speed.

Equations (11) and (12) give the liquid crystal director response time for a uniform phase profile, in contrast to an optical response from the more complex steering profile required in an optical phased array. Nonetheless, the quadratic scaling of response time with thickness seems to roughly predict device state-to-state steering performance. A reflective device geometry may be used to achieve a beam doublepass that minimizes the required liquid crystal thickness, and hence minimizes the time for director decay given in (11). Reflective steering at visible wavelengths ($\lambda = 532$ nm) then leads to 3 ms switching times using liquid crystal E-7 at room temperature. Since an optical array requires a liquid crystal layer of thickness $t = \lambda/\Delta n$ to achieve a 2π phase shift, we may use (11) and identify the quantity $(1/\tau_d) \propto \kappa(\Delta n)^2/\gamma$ as a merit factor [35] that characterizes the switching speed of a liquid crystal. Elevating the temperature will decrease the γ/κ ratio for a liquid crystal. This may lead to a larger (optimum) merit factor at some higher temperature since competing changes in Δn are small until the temperature approaches the neighborhood of the clearing transition. For example, the liquid crystal PTTP-33 was found [36] to have a merit factor at 114°C that is 12 times that of the room temperature E7 used in the present steering experiments. Room temperature eutectics of such materials are thought to be possible. It is apparent that significant improvements in the state-to-state switching times for optical phased arrays may be possible through the use of new liquid crystal materials.

Table 1 The Effect of Increased Liquid Crystal Birefringence on Beam Switching Time, as a Function of Wavelength

Birefringence	Response time at 1 μm	Response time at 5 μm	Response time at 10 μm
.2	4 ms	100 ms	400 ms
.4	1 ms	25 ms	100 ms
.6	440 μs	11.1 ms	44.4 ms
.8	250 μs	6.25 ms	25 ms
1.0	160 μs	4 ms	16 ms

These response times are much slower than are now available for microwave phased arrays. However, at shorter wavelengths they already compare favorably with the quasi-agile mechanical steering options currently available for laser radar. At longer wavelengths additional development is required to surpass the speeds of current mechanical options. Basic methods of improving speed are:

1) Decrease liquid crystal layer thickness and increase speed by the inverse square of the thickness. There are a number of techniques to do this, which will be discussed below.
2) Decrease liquid crystal viscosity. This can be done by developing new materials, or by operating at elevated temperature. Increasing the temperature of a liquid crystal has been shown to decrease the switching time significantly [37].
3) Increase the driving voltage used to impose switching.
4) Improve liquid crystal alignment techniques.
5) Adopt ferroelectric liquid crystals which are inherently faster in their response, on the order of microseconds [38].

There are a number of methods to decrease the thickness of the liquid crystal layer. The simplest is to use a material with higher index of refraction. Table 1 shows the influence of increasing index of refraction from 0.2 to higher values while leaving all other parameters constant. Table entries are scaled from a baseline 4 ms response time for a transmissive phased array at a wavelength of 1.06 μm. The minimum phase shifter thickness scales linearly with birefringence; hence the response time decreases quadratically with birefringence. Materials with birefringences of the order of 0.4 are certainly possible with careful molecular engineering, as has been advocated by Wu [39]. Possibilities for materials with even higher birefringence exist [40]. The performance payoff for advanced materials will be significant.

Another technique to realize a thinner liquid crystal layer is to have the light pass through the liquid crystal layer more than once. The reflective-mode operation in which light passes through the liquid crystal layer twice has already been discussed. If a resonant-mode phase shifter design is

used, a transmitted wave effectively experiences multiple passes through the liquid crystal layer, the equivalent number depending upon the Q of the resonator. This approach is particularly attractive for longer-wavelength applications. For example, a 10 μm laser beam making 10 passes through a given liquid crystal layer experiences a phase shift roughly equivalent to that for a 1 μm laser beam making a single pass, with the same short-wavelength response time. Using the resonance design to allow a long wavelength laser radar to have the speed of a short wavelength system leads to manufacturing tolerances which have already been successfully demonstrated. The resonance phenomenon, however, is inherently narrow band. As an example, the phase shift, Φ, on reflection from a Gires–Tournois etalon is given [41] by

$$\tan\left(\frac{\Phi}{2}\right) = \frac{(1+\cdots\overline{R})}{(1-\cdots\overline{R})}\tan\phi \qquad (13)$$

where R is the intensity reflectivity of the partially transmitting front surface, and ϕ is the phase change from a single pass through the media. In the limit of vanishing R, Φ reduces to 2ϕ, the round-trip phase shift. This is the case of a reflection-mode optical phased array. The fractional expression in (13) is a resonant enhancement factor. As R increases, Φ is substantially increased for the same ϕ. The dispersion, however, also increases. At resonance (ϕ = any odd integer $^*\pi$), the phase dispersion is strongest, and the bandwidth most limited. This is not necessarily an issue for a narrowband laser-based system. However, for passive acquisition systems, discussed later, this can be a substantial issue.

Encapsulation of a liquid crystal in a polymer matrix is an alternate means to achieve faster switching speeds. The encapsulated liquid crystal experiences an effective liquid crystal thickness of the order of the size of the encapsulating cells, which can be orders of magnitude smaller than the overall thickness of the film. Encapsulated liquid crystal systems have been demonstrated for displays [42]. There are tradeoffs to this approach, however. The bubble size must be kept much smaller than the wavelength of light used in order to minimize scattering. When the bubble size is small, high voltage is required to re-orient the liquid crystals, owing to the proximity of the liquid to a surface. The effective birefringence is reduced in proportion to the fraction of encapsulated cell volume to encapsulating polymer volume (the fill factor). Furthermore, Δn is reduced to $[(2n_o+n_e)/3-n_o]$ instead of n_e-n_o. For both of these reasons, a greater thickness of encapsulated liquid crystal is required to achieve a given change in effective index.

A thinner liquid crystal layer can be used with an input prism over the liquid crystal layer to effect propagation more nearly in the plane of the liquid crystal. This allows the requisite λ/Δ waves of material to be sampled in a thinner-than usual film of liquid crystal [43]. A unit using this design has been fabricated, achieving the design value of times six reduction in response time for operation at 10.6 μm.

Ferroelectric liquid crystals have been shown to exhibit much faster switching times than nematics; however currently available materials are binary in their phase response whereas a grayscale phase shift capability is required for phased array applications. A multiple layer structure of n binary devices having thicknesses $2\pi/n$ could be used to provide the needed gray scale; however this would be a much more complex structure to fabricate. For practical applications, it is preferable to await the development of true grayscale capable ferroelectrics, which are being pursued [20]. The smectic A^* electroclinic phase offers fast response and inherently analog phase variation via the rotation of the director with applied field. Although the phase range is currently materials limited, a smectic A^* small-aperture phase retarder has been operated as a half-wave plate with a voltage-addressable fast axis [44]. Use of an asymmetric Fabry–Perot cavity should in principle allow fabrication of a full-wave phase shifter using available materials [45]. Newer smectic $A*$ liquid crystals should be capable of full-wave phase shift, eliminating the need for the resonator [46]. However, considerable development is required to achieve large-aperture optical phased arrays having the microsecond response times promised by ferroelectric approaches.

D. Reduced Leadout Addressing Architectures

The leadout requirements dictated by the data in Fig. 11 are challenging, even for 1-D optical phased arrays. However, high-density flat-panel displays using multiplexed addressing and on-board integrated circuitry are now reaching the million pixel level, which would suffice for a 1-m aperture at a wavelength of 1 μm, and more than suffice for a 1 m aperture at a wavelength of 10 μm. Although the addressing circuitry for liquid crystal based optical phased arrays is in principle similar, there are additional addressing requirements which preclude direct adoption of these display circuits. The refresh rate of most multiplexed display addressing schemes is designed to make use of the persistence of the human eye. It is acceptable that the voltage at each pixel of a display be allowed to droop somewhat during the refresh cycle. This is generally not the case for an optical phased array which is supporting a sensor. Variation of the voltages on the individual phase shifters during a refresh cycle would cause both the beam intensity and the side-lobe levels (but not the beam direction) to vary. To circumvent this, custom addressing has been developed for optical phased arrays, incorporating sample-and-hold circuitry to maintain the individual phase shifter voltages during array refresh cycles. This addressing circuitry currently can handle several thousand independent channels. A hard-wired subarray architecture has been implemented to reduce the leadout requirements to match the available addressing capability.

Fig. 12 illustrates the multiple-state beam steering concept. The 1-D aperture is divided into many identical subarrays. Address lines are used to connect in parallel the corresponding phase shifters of each of these subarrays. The figure illustrates the case of only six phase shifters

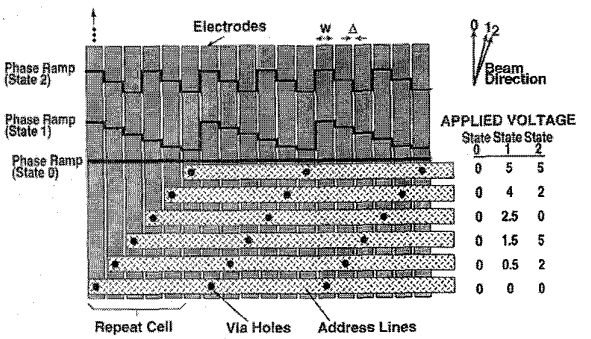

Fig. 12. *Multiple State Beam Steerer.* Multiple state architecture is used to further reduce addressing requirements. The phase shifters are divided into subarrays and corresponding phase shifters in each subarray connected in parallel. The same voltage pattern is imposed on each subarray. This limits the number of directions to which the array can steer.

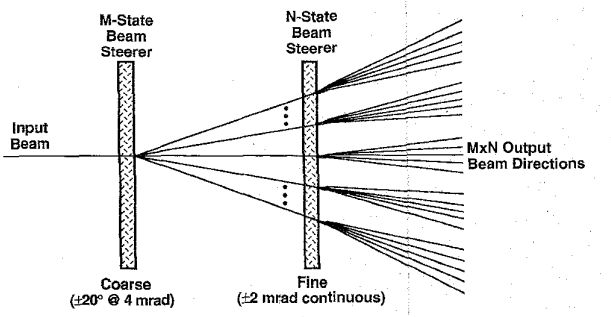

Fig. 13. *Cascaded course/fine beam steering architecture.* Full angular addressing flexibility is recovered, even using multiple state addressing for the course beam steerer, by using a course/fine architecture. The fine beam steerer is fully addressable, but only steers over a small angle.

per subarray, an example chosen for ease of illustration. In actual practice, hundreds of phase shifters are used for each subarray. Specifically, a 4.3×4.1 cm array demonstrated at Raytheon in 1991 consists of 43 000 phase shifters divided into 168 subarrays with $m = 256$ phase shifters in each subarray. As schematically depicted in Fig. 12, application of a voltage profile to the address lines causes the voltage profile to be repeated periodically across the entire aperture. Thus this architecture reduces the number of phase shifter interconnects to the number of phase shifters chosen per subarray, regardless of the total number of phase shifters on the entire aperture. In this way, the number of control leads for an entire optical phased array can be significantly reduced (from 43 000 to 256 in the above case).

This architecture is referred to as a "multiple-state beam steerer" because the number of addressable beam steering states is limited to a discrete, noncontinuous (comblike) subset of the angular directions available from a fully addressable array. Each "state" results in steering to a discernibly different direction, well separated in angular space from adjacent states. The available steering directions are determined by the number of waves of phase shift programmed across each subarray.

The number of steering states for a multiple-state steerer depends on the subarray size. Two staircase phase ramps are illustrated in Fig. 12. These are the only allowable phase distributions (for steering to a given directional sense) for that simple case. The three-phase-shifter periodic phase distribution shown corresponds to the minimum number of phase states required to define an asymmetric profile. That is, a three-phase-state period is required to unambiguously define a steered angle. A three-phase-shift period gives the largest possible steering angle, but the coarse three-level quantization would give a low steering efficiency (68%). A two-level phase period is a symmetric phase distribution which steers with equal efficiency into both positive and negative directions. The six-phase-shifter phase distribution illustrated is the largest allowed period for the example shown in Fig. 12 and corresponds to the smallest steering angle.

Each ramp inside the subarray does not need to have the same period (the number of steps in the ramp). Across a subarray however there must be an integral number of 0 to 2π phase ramps. The maximum number of phase ramps across the subarray is the number of phase shifters in the subarray, m, divided by 3, the steepest allowed unambiguous phase ramp. This is also the maximum number of steering angles to one side of an unsteered beam. The maximum number of angles that a subarray architecture beam steerer can steer to is approximately $M = (2m/3+1)$. This compares to a fully addressable array, which can steer to $M = (2D/3d + 1)$ states, or angular positions, where D is the full aperture and d is the size of an addressable phase element. For a subarray with $m = 17$, five ramps of 2π phase shifts are the largest integer number of full ramps possible. This corresponds to phase ramps with 3, 4, 3, 4, and 3 steps, respectively. In order to avoid significant phase walk off it is important to alternate between the nonequal number of steps in the phase ramps. For a practical situation one would not tend to chose the $m = 17$, as in the example. Non-prime numbers, which allow equal period phase ramps even at large steering angles are preferred.

Although the number of steering states for an array is decreased by use of the multiple-state architecture, complete steering flexibility can be recovered through use of the fine/coarse architecture discussed below. Thus the multiple-state steering design imposes no limitation. It is however essential for the fabrication of optical phased arrays having useful apertures, given currently available addressing technology. The design, operation, and addressing of multiple-state beam steerers has been described in detail previously [47]–[50].

Fig. 13 illustrates a fine/coarse-steering optical phased array architecture that can achieve the same number of addressable steering states available with a fully addressable array, but without the large number of leadouts ordinarily required for a fully addressable array. Cascading of an M-state array with an N-state array allows up to $M \times N$ directions to be addressed, as is depicted schematically. The number of leadout required to address this large number of angles is however just $3(M + N)/2 - 3$.

The M-state device is a multiple-state array of the type described above, and is denoted here as a "coarse" beam steerer. The N-state device, denoted here as a "fine" beam steerer, is designed to have a small FOV, meaning that both the spacing, d, between phase shifters and the array size ($D = nd$) are large compared to the wavelength. The number of phase shifters on the (full) aperture can then be small enough to allow independent addressing of every phase shifter with modest leadout counts. The N-state device is chosen to have only a single subarray, and a manageable number of control leadouts. If the minimum steering angle (the step size) of the (coarse) M-state device is designed to match the half-FOV of the fine steerer, spot-to-spot "continuous" steering coverage over the full FOV of the coarse array is obtained. The fine steerer thus "fills in" all beam directions between the coarse steerer steps.

Fig. 13 refers to the specific case of a continuous fine steerer with a 4 mrad FOV and a coarse steerer with 4 mrad steering steps. This design has been implemented with a coarse steerer having $m = 256$ phase shifters per subarray and a fine steerer having $n = 512$ phase shifters. The number of leadouts required to control the cascaded combination is just $m + n = 768$, as compared to the 40 000 which would be required for a single, fully addressable array having the same number of addressable beam directions.

This approach is analogous to the common use of cascaded fine/coarse galvo-scanners to enhance the "resolution" of mechanical beam steerers. Cascading phased arrays has not previously been suggested or demonstrated, quite possibly because it is not needed for (fully addressable) microwave arrays. Although the figure illustrates the case of transmissive devices, the fine/coarse cascading can be implemented with reflective devices or a combination of reflective and transmissive devices.

E. Angular Tracking Accuracy, Adaptive Optics, and Multiple Beam Applications

The number of steering directions programmable with a "fine" array is actually considerably greater than the classical Rayleigh resolution of $N = (2n/3 + 1)$, which only counts the number of diffraction limited, or Rayleigh, spots that can be addressed. Each wave of phase gradient across a filled phased array aperture steers a beam exactly one Rayleigh spot size. A fully addressable optical phased array is capable of essentially continuous steering since it can be made to steer with fractional-spot-size angular positioning by programming fractions of a full wave of phase gradient across the aperture. Such "super-Rayleigh" position angular accuracies are commonly obtained with microwave phased arrays, for which the fine steerer is a true analog. Steering to one-hundredth of a spot size already has been demonstrated with moderate aperture optical arrays. For a 20-cm aperture beam steerer operating at 1.06 μm, the resultant steering accuracy would be approximately 65 nrad. Such a steering angle requires a phase ramp of 0 to $2\pi/100$ across the aperture of the steering array, which in turn requires an analog phase adjustability of about 0.01 rad (0.6°), assuming six phase steps are needed to approximate a reasonably smooth phase ramp. This precision is obtainable with the phase shifters and drive electronics already developed. Nanoradian steering accuracies are not possible with any other known agile optical steering approach. Optical phased arrays can steer to very precise positions, since the pointing position is determined by specific electrode spacings, just as in a fixed grating structure. Any mechanical system attempting to point to an accuracy on this order would most likely require complex closed-loop control and heavy, bulky structures to implement. Precise pointing, using mechanically simple systems, is one of the strong features of optical phased array technology.

Blazed grating profiles have been emphasized here since the primary goal is direction of maximal beam energy into a particular angular direction. However, these optical phased arrays can also be used to create other dynamic diffractive optical elements, without any hardware modifications. For example, Fresnel lenses [51], [52] and fanout gratings can be programmed directly onto the array, allowing laser beams to be focused or fanned out into multiple beams.

A 1-D optical phased array can be programmed with a cylindrical parabolic Fresnel lens, having phase profile specified as

$$\Phi(x) = (\pi x)/(\lambda f) \bmod (2\pi) \tag{14}$$

where λ is the beam wavelength, f is the lens focal length; and x is the distance from the lens optical axis. The lens can be converging or diverging, with continuous control over f. Two such arrays form an axially symmetric parabolic lens. If the programmed focal length is too short, the peripheral Fresnel zones may be undersampled, giving rise to aliasing effects which can degrade the quality of the focused beam. This condition can be expressed in the following form:

$$f_{\min} = \frac{Dd}{2\lambda} q_{\min} \tag{15}$$

where $f_{\min}$ is the minimum focal length; D, the beam diameter; d, the phase shifter spacing; and $q_{\min}$, the number of phase steps per modulo 2π phase ramp. In the case of lensing, $q_{\min} = 4$ is often found to be adequate. Expression (15) is equivalent to the statement that the smallest feature size of a Fresnel lens is $2\lambda F$, where $F = f/D$, with the feature size for a gray level device taken as $q_{\min} d$.

Fanout profiles are generally not calculable in closed form. Computer-optimized profiles are stored as state-vector files and retrieved when a beam fanout is to be programmed onto the phased array.

Examples of dynamic lensing and fanouts achieved with the current optical phased arrays are shown in Section V. The programmable, dynamic nature of the diffractive element offers significant advantages over fixed element systems. Dynamic pointing and focus control enables real-time compensation in optical systems that experience variations

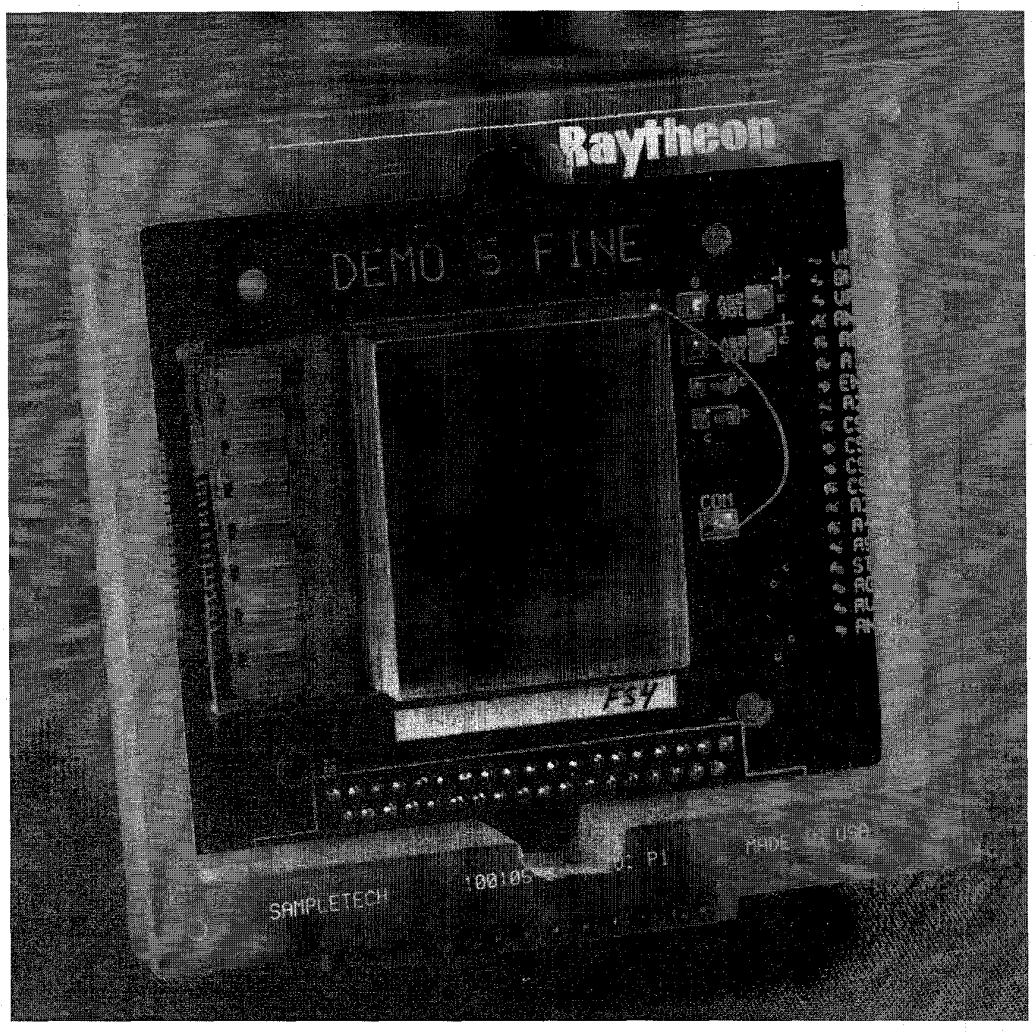

Fig. 14. Photo of a 4 cm× 4 cm fine angle beam steerer.

with temperature or other environmental variables. Such control will also be useful for auto-alignment in systems for which it may be difficult or impossible to maintain alignment manually.

V. Optical Phased Array Experimental Results

Currently available optical phased array hardware is described in this section and performance levels achieved to date are discussed. Anticipated future performance potentials are also discussed.

Fig. 14 shows a prototype optical phased array fabricated for steering of Nd:YAG laser beams. This "fine" steering array has a 4 mrad nominal field of view and an active aperture of approximately 4 cm square. The "coarse" arrays are similarly fabricated and packaged. These are reasonably well engineered prototype devices, but have not yet been optimally packaged for compactness or for environmental stability. The arrays are typically mounted directly on the printed circuit boards which interface the input cable to the addressing chips, as shown here. Future devices can be more compactly packaged with both azimuth and elevation devices on a single substrate, and both "fine" and "coarse" (2-D) units mounted in a single package.

Drive and control of the arrays is currently realized via custom built electronics resident within an 80486-based EISA bus computer. Under software control a serial analog data stream is generated together with digital address and control lines to control up to 1536 independent channels. This is sufficient to fully control two "fine" arrays and two "coarse" arrays of the current design, one each for azimuth and elevation. The addressing architecture is modular. Multiple 1536 channel circuits can be controlled from one computer, and each circuit contains six independent 256 channel analog data streams generated in parallel. Although the arrays themselves can not yet react faster than about a millisecond, the driver electronics have been designed with future, faster-switching devices in mind, and will support updates of the steering direction every 88 μs, an 11.3 Hz refresh, or frame, rate. The voltage range for each channel in a serial train is effectively 10 V^{rms} with

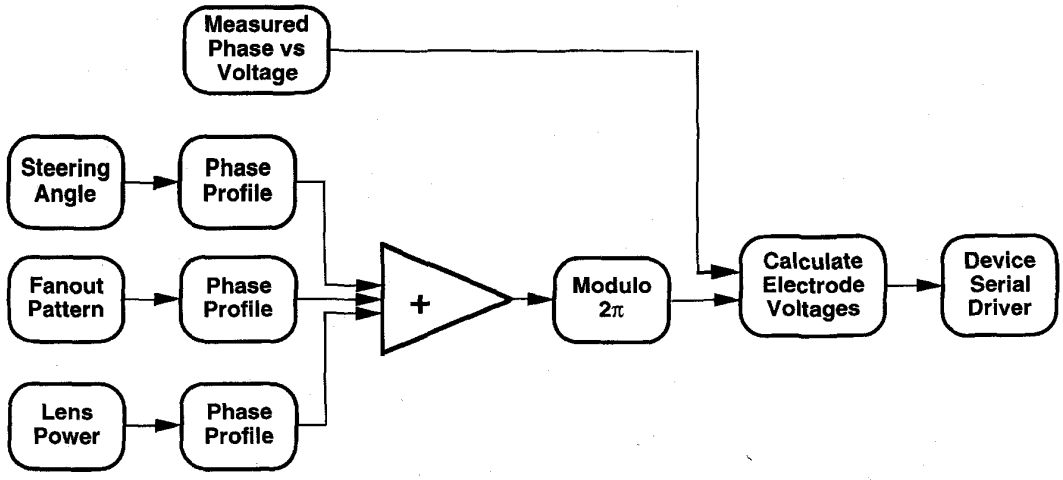

Fig. 15. Open loop voltage/phase specification algorithm.

a 10-b resolution. The circuit cards each occupy one LISA bus slot, are 4.5″ high by 8.5″ wide, and weigh 8 oz. The design is such that the card can be replaced by four custom integrated circuit chips at a future date. Connection to a beam steerer interface is presently made through a 37 pin cable connector, visible on the lower edge of the package. Sophisticated graphical user interfaces (GUI's) communicate with the drivers via high level language software. These GUI's are employed to both optimize and demonstrate device performance. A 16-steering state RAM buffer is employed by the serial driver software as a cache to eliminate high level language bottlenecks.

The control electronics have recently been adapted to conform to an Ethane communications protocol. These modifications have allowed the parallel development of a lightweight, compact, and portable demonstration unit wherein the optical phased array can be controlled using subnotebook size computers, such as the HP Omnibus. Using the standard 10BaseT Ethernet link and the slow ISA bus interface currently furnished with subnotebook sized computers degrades the frame rate to about 500 Hz. However, this speed penalty should soon be eliminated with the advent of PCI bus systems for notebook computers and high speed 100BaseT Ethernet links.

Data generated by the control electronics is input to serial-to-parallel silicon integrated circuits which store and present the analog data to the beam steering device. These custom chips are mounted directly on the steering array and can be seen adjacent the left side of the aperture. Each chip contains 64 independently addressable sample and hold outputs with a 10 V^{rms} range. The circuit design integrates analog and digital circuitry onto a 3 mm × 7 mm silicon chip. Four chips are grouped with each serial data train such that all 256 voltages stored in each group are output in parallel using a strobe signal. All phase shifters on a steering array are switched simultaneously when a new steering direction is requested. This architecture is scaleable to any number of output channels with no increase in refresh time (agile switching time). Designs for 256 channels on a single chip with an even smaller footprint have been shown to be feasible with available technology.

A. Computerized Control of Beam Steerers

The large number of independently addressable phase shifters must be properly adjusted for high performance phased array operation. Automated computer optimization of the required voltage levels has been implemented for that purpose. An open loop algorithm is shown in Fig. 15. The phased array is precalibrated by measuring its phase retardance versus voltage characteristics, using interferometric techniques [53]. During initialization this information is retrieved, along with any requested fanout phase profiles, wavelength λ, the phase shifter spacing d of the specific array, the desired steering angle θ, the fanout spatial frequency Λ, and the lens dioptric power $1/f$, if desired. The requisite phase profiles are calculated as follows:

1) beam steering phase profile:

$$\Phi(i) = (2\pi di/\lambda)\sin\theta \tag{16}$$

2) fanout profile:
   Determined via simulated annealing algorithms [54]
3) lens profile:

$$\Phi_L(i) = \frac{\phi}{\lambda f}\left\{d\left(i - \frac{N}{2}\right)\right\}^2 \tag{17}$$

where N is the number of electrodes and i is the consecutive electrode number. The composite phase profile is obtained by summation,

$$F(i) = [\Phi_S(i) + \Phi_F(i) + \Phi_L(i)] \bmod (2\pi). \tag{18}$$

$\Phi(i)$ is converted into a voltage profile by linear interpolation of the measured phase versus voltage

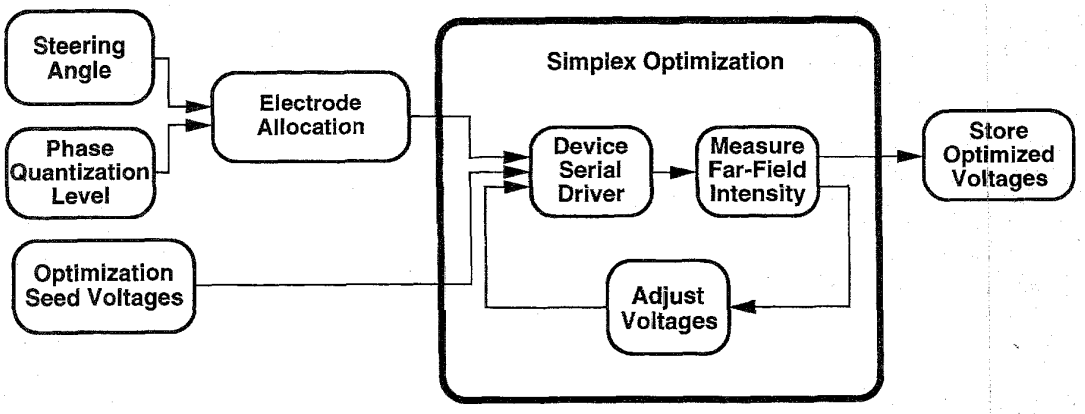

Fig. 16. Closed loop voltage/phase optimization algorithm.

characteristic of the device, and the resultant profile is routed to the device controller board for generation of the corresponding voltage pulse train. This procedure is effective for real-time control of the "fine" arrays.

For "coarse" arrays, the very fine phase shifter spacings generally result in unavoidable cross talk between adjacent phase shifters, in which case it is difficult to accurately calibrate the individual elements. In this case the closed-loop optimization algorithm shown in Fig. 16 is used. As a "seed" voltage profile, the best available guess is used. This may be the profile for an adjacent steering direction, interpolated for the new direction, or simply a linear voltage profile having the proper periodicity for steering to the desired direction. The seed profile is applied to the array, the resultant beam profile acquired from a line scan camera, and the peak intensity determined for the desired direction. A downhill simplex optimization algorithm is used to iteratively maximize the beam intensity as a function of the independent voltage variables. When the maximal intensity is obtained, the optimized voltages are saved to a file together with the other relevant data. A typical "cold" optimization run is shown in Fig. 17. The 500 iterations shown here take several minutes on an 80486 PC. Fig. 18 shows the far-field intensity pattern for the initial seed profile and the resultant optimized profile. The example was run with a particularly poor seed choice to demonstrate the robustness of the algorithm. With "better" seed choices, the procedure is faster. This entire optimization procedure need be done only once for each array.

Fig. 19 illustrates typical steering performance for a transmissive-mode "fine" steering array designed for 1.06 μm operation at 1.06 μm. Measured normalized far-field intensity (steering efficiency) is plotted versus steering angle over the designed half-field of view of 2 mrad. The intensity profiles have been sampled with a calibrated 1×1000 linear detector array, using a 1.06 μm laser beam. The unsteered Gaussian input beam profile (device "off") is shown by the dotted intensity profile at boresight. Representative profiles for beams deflected by 50 μrad, 830 μrad, and 1667 μrad are also plotted as overlays, which can be done here without confusion owing to the almost complete lack of sidelobes. The single input beam is seen to be efficiently converted to a single output beam with high efficiency and no visible sidelobes. All beams are diffraction limited to within measurement accuracy. The 50 μrad steering angle shown is by no means the smallest possible; the device is actually capable of submicroradian steering. The dotted line directly above the profile envelopes represents the theoretical steering efficiency fall off due to the quantization of the desired linear phase ramp by a digitized stepwise approximation [23] as expressed in (2). The deflection to 1667 μrad uses approximately eight phase steps per full wave of phase ramp, which corresponds to a theoretical efficiency of 95%; the measured efficiency is 93%. The device can be operated well beyond its nominal design field of view. Measurements out to 4 mrad (double the design field of view) have been made, showing efficiency falloffs in accord with the above phase quantization error. In addition to the relatively small efficiency losses, these devices have relatively low insertion losses of about 5%. There is virtually no absorption loss contribution from the liquid crystals in the near infrared and visible spectra. The measured insertion losses are due primarily to imperfect thin-film coatings of the various device interfaces and are expected to fall as the fabrication technology matures. It also should be noted that, if desired, these "fine" steering arrays can be designed to have either much larger fields of view or even higher efficiencies at the design steering limits; the number of driver channels need simply be increased.

Fig. 20 shows a typical "antenna pattern" for a "coarse" steering array, also designed and fabricated for 1 μm operation. Microwave engineers usually prefer such logarithmic plots to characterize the sidelobe performance of a phased array. The array has been programmed to steer the incident beam to approximately 1.5°. The largest "sidelobe" for the optical phased array is the residual beamlet at boresight, which here is approximately 17.5 dB down from the peak steered beam intensity, and represents the unsteered portion of the incident beam. It is a consequence of an imperfectly programmed phased profile. There is also an image lobe

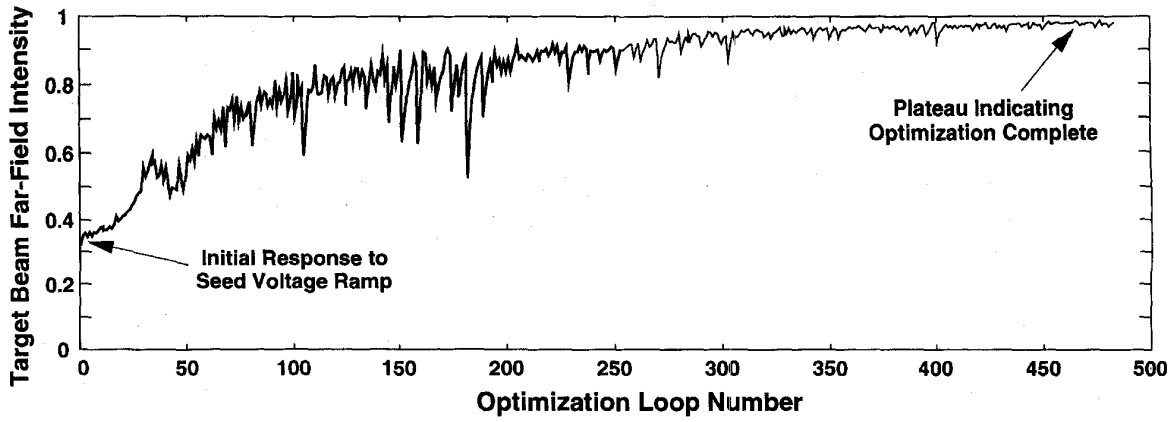

Fig. 17. Typical "cold" optimization run.

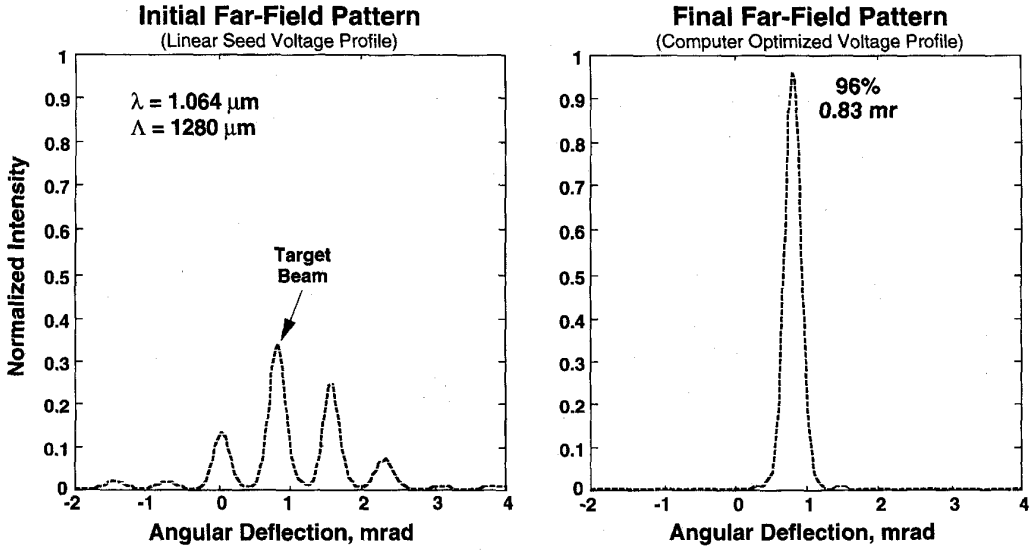

Fig. 18. Far field intensity pattern for the initial seed profile, and the resultant optimization profile.

at the negative of the steering angle which is about 18 dB down. All other sidelobes are more than 20 dB down. For the data shown, almost all of the energy seen below −20 dB is actually detector noise. The actual steering efficiency for this device is about 85% at this angle. Steering to angles as high as 10° has been demonstrated with similar coarse steering arrays; however, the steering efficiency of current units falls off quickly beyond 5° due to limitations of the lithography and liquid crystal material in current use. Modeling suggests that more optimally designed and fabricated devices should be capable of steering to several times these angles with high steering efficiency.

The optical phased array is inherently a high-resolution, high-precision device. The beam steering angle is determined by the grating equation and depends only on wavelength, angle of incidence, and the (electronically programmed) grating period. The grating period can be programmed to very high accuracy. A 2π linear phase gradient across an aperture D (or across the input beam width D, whichever is smaller) steers an input beam by exactly one Rayleigh spot in the far field, $\theta = \alpha\lambda/D$, where a is the near-unity aperture constant and is fixed by the input beam spatial profile and aperture shape. For a uniformly filled 20-cm circular aperture at 1.06 μm, $\theta = 6$ μrad. Steering to larger angles corresponds to programming multiple waves of phase gradient across the aperture, one for each Rayleigh spot. Smaller phase gradients correspond to steering by less than full Rayleigh spot increments, the steered angle being strictly proportional to the programmed phase ramp. As discussed above, present generation addressing electronics allow the adjustment of phase shifters to about 0.01 rad (10 bits voltage resolution), which is adequate for efficient addressing of a 1/100 phase gradient and a corresponding steering angle of only 60 nrad.

Fig. 21 demonstrates microradian-precision steering over a ± 100 μrad field. Measured output angle position is plotted versus the programmed input angle. Similar performance is obtained over the entire field of view. The response

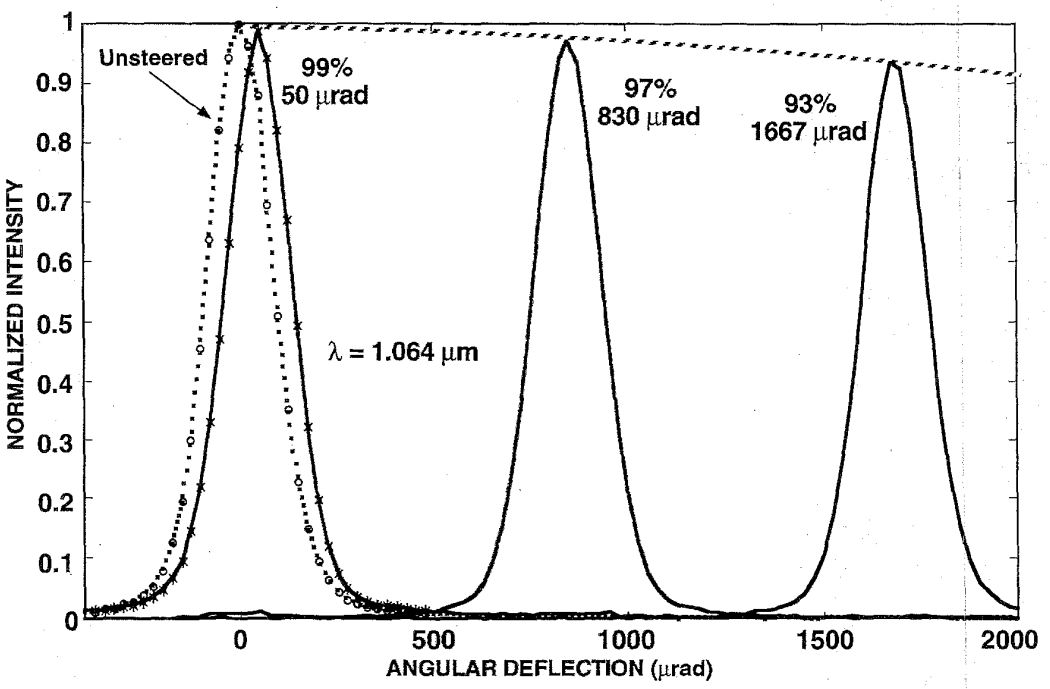

Fig. 19. *Fine angle beam steering data.* High efficiency steering, with virtually no sidelobes, is shown by the fine angle beam steerer. The steered beams are diffraction limited to within measurement accuracy.

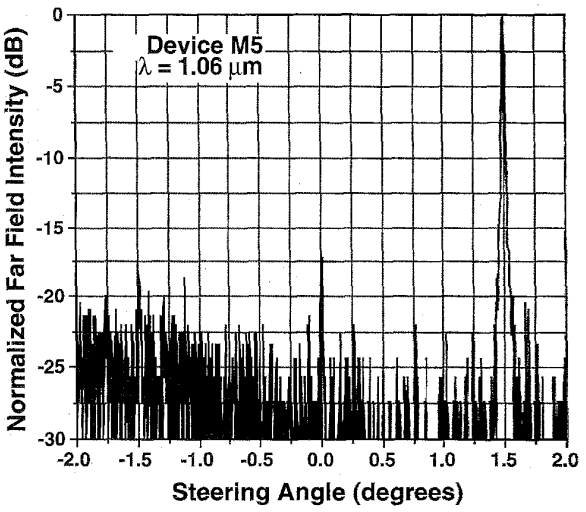

Fig. 20. Typical "antenna pattern" for a course beam steerer. This pattern is plotted on a semilog scale, so it is possible to see the sidelobes. Detector noise however is significant at about the −20 dB level, making it impossible to see where the real sidelobe level is below −20 dB.

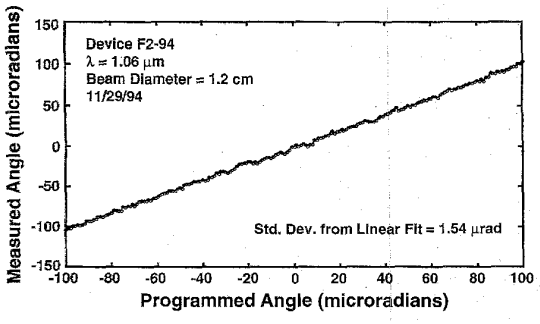

Fig. 21. *Microradian precision steering.* This chart shows beam steering to almost one hundredth of a diffraction limited spot size. The setup had a 1.5 μrad measurement noise floor.

is linear (with unity slope) within an rms angular noise (standard deviation) of approximately 1.5 μrad, which is the measured noise floor of the current measurement system with the beam steerer off. The input beam diameter is approximately 1.2 cm with a corresponding Rayleigh spot size of approximately 100 μrad. These data therefore represent steering to one-hundredth of a Rayleigh spot. The sub-Rayleigh motions are measured by tracking the centrum of the beam intensity as registered on a CCD array; some of the system noise is thought to arise from pixel nonuniformities in the array. Scaling the data from a 1.2 cm beam to a 20 cm beam would yield tracking accuracies better than 80 nrad. While other challenges would have to be overcome to use a 20 cm array in such a fashion, this is an astounding potential tracking accuracy for a mechanically simple system.

There is no observable jitter or hysteresis on the beam motions down to the 1.5 μrad measurement limit, and at this level none is expected for a phased array. Nanoradian resolution and precision should be feasible. The measured steering positions are strictly repeatable, within the system noise level. It is expected that a more sophisticated

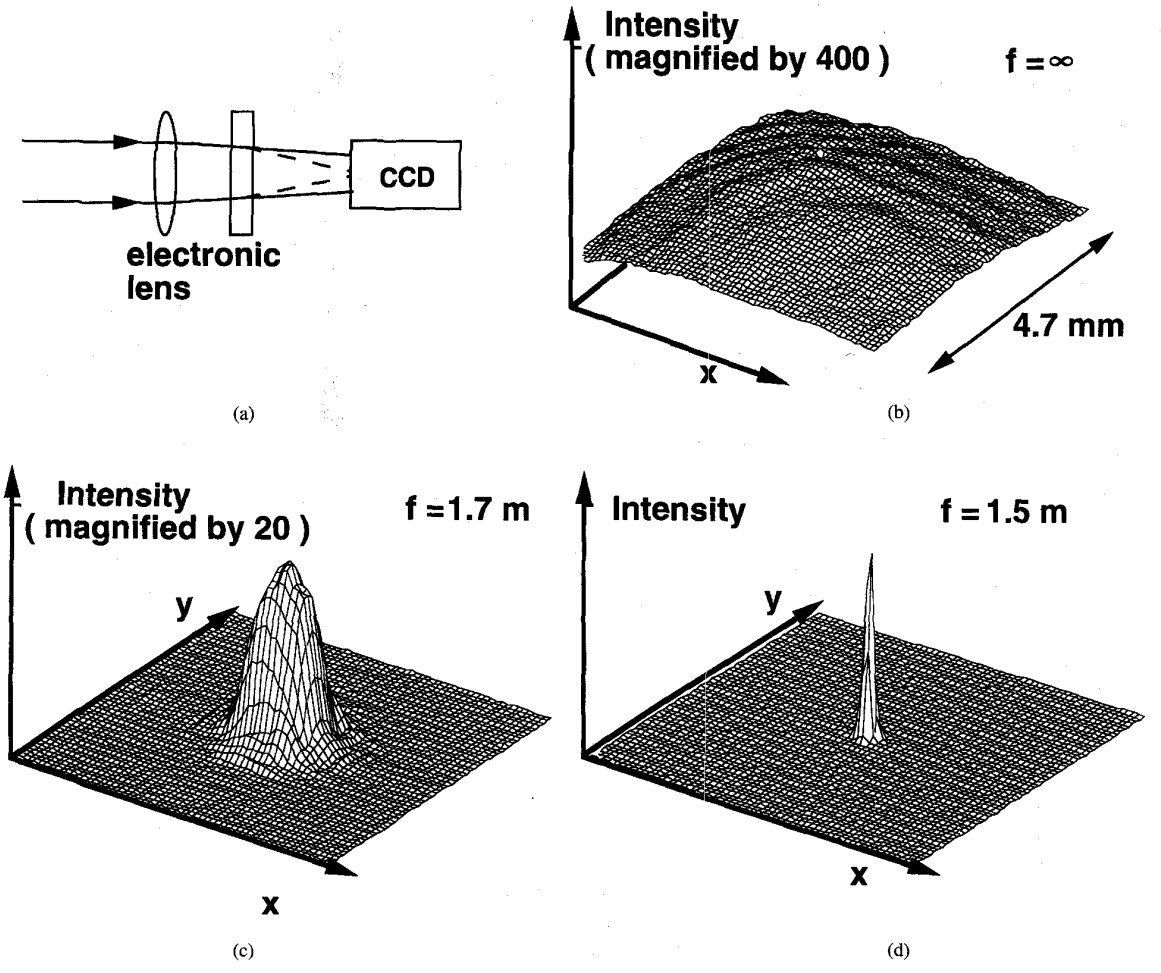

Fig. 22. *Electronic lensing demonstration.* This data shows beam lensing, using only the optical phased array with a suitable imposed phase profile.

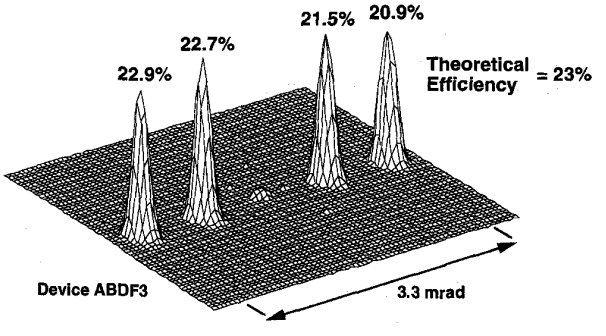

Fig. 23. *Demonstration of four beam symmetric fanout.* With a suitable imposed phase profile multiple high quality beams can be created from a single beam.

measurement system would demonstrate even higher performance steering parameters. It should be noted that all data are taken strictly open loop. There is no need for angle sensing resolvers or encoders with a phased array beam steerer. All beam directions are precisely determined (by the programmed grating) with respect to the device boresight within the precision of the lithographically formed electrode structure, which has parts-per-million accuracy. The dynamic range of an optical phased array is seen to be very high. Steering to $\pm 5°$ by 60 nrad steps corresponds to approximately 3×10^6 programmable, discernible, beam positions.

Fig. 22 demonstrates the measured electronic lensing of a Nd:YAG laser beam. A nearly collimated beam propagates through the phased arrays and onto a CCD camera, as shown schematically in (a). The initial beam intensity profile with the phased array "off" is shown in (b). The Gaussian profile of the nearly centered beam can be seen. A partially focused intensity profile is shown in frame (c) for the case of the electronic lens adjusted for a 1.7 m focal length. Frame (d) shows the intensity for an electronic focal length of 1.5 m, which essentially focuses the beam on the CCD array. Within a measurement limit of about 1.2 times diffraction limit, the electronically focused beam is diffraction limited. The intensity has been increased nearly 1000-fold, with no apparent aberrations. Arrays can be designed to provide considerably shorter focal lengths; however, 1 m is the limit for the device demonstrated here.

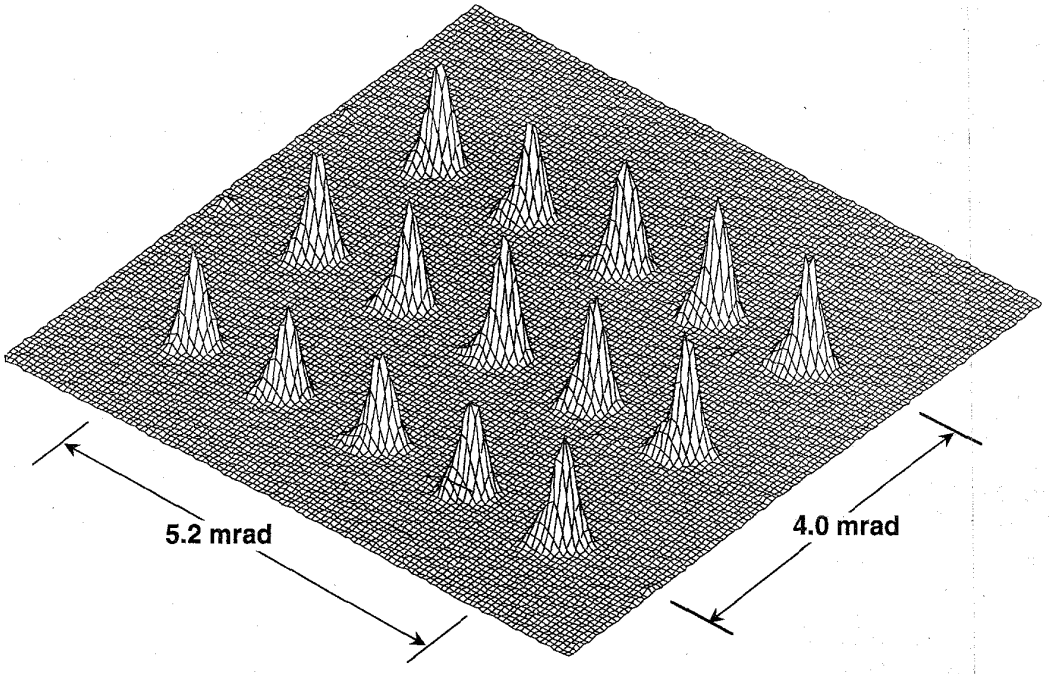

Fig. 24. 3×5 beam fanout pattern. By using crossed gratings a single beam can be transformed into a 3×5 beam pattern.

Fig. 23 demonstrates the fanout capability of the phased array. Such multiple beam fanouts may be generated by programming phase profiles optimized for such purpose [55]. A single space-fed input beam is then split into an arbitrarily chosen number of output beams, here four. The intensities of each output beam can be independently chosen; equal intensities are often desired, as has been programmed here. The example shown is a so-called asymmetric pattern, with the central beam deliberately omitted. A multilevel phase profile has been programmed to provide higher uniformity and eliminate sidelobes. The data have been normalized to the single beam intensity transmitted through the device when programmed with a uniform phase profile, in which case there is an 8% insertion loss for this device. Thus 81% of the total incident power is directed into the four desired diffraction orders. The optimal phase profile was calculated using a simulated annealing algorithm. The optimal efficiency found for a phase-only device is 23% coupling to each direction; hence, the device is exhibiting 96% of the theoretical diffraction efficiency.

Such one-to-N splitting functions may be useful for generating efficient search patterns for laser radar, and has also received attention as one means to implement space-fed optical switching networks with multiple interconnect capability [56], [57]. Most fanout work has in fact been in this latter field. Fanout phase gratings are typically optimized subject to practical restrictions on the number of phase levels available. The early work of Dammann noted that fixed binary gratings were the easiest to realize, but that the more general multiple-level phase gratings would yield significantly higher overall efficiency. Experimental work using programmable phase apertures has involved both approaches. For example, programmable binary phase fanout profiles have been demonstrated using ferroelectric liquid crystal spatial light modulators [58], showing a 9% intensity transmission and relative diffraction peak heights close to theoretical. In a demonstration of arbitrary phase profiles, pixelated nematic liquid crystal displays have been operated in the electrically controlled birefringence mode to create fanouts with a 15% overall diffraction efficiency [59]. These efficiencies are significantly lower than is available using the current optical phased arrays.

Two-dimensional fanouts can be realized by cascading two 1-D arrays. Fig. 24 illustrates a 3×5 pattern so generated. By merely altering the repeat period of the applied phase profile it is possible to change the field of view encompassed by the pattern. This effect is shown in Fig. 25. It is also possible to combine beam fanouts with the focus and steering functions by merely adding the appropriate phase profiles (modulo 2π). This is illustrated in Fig. 26 in which the phased array creates the 5×5 fanout (a) and acts as its own transform lens to form the far-field pattern shown. When the programmed lens power is decreased, as in (b), a rectangular far-field pattern is formed that is nearly space filling. In either case the entire fanout pattern may be redirected to a different central angle by adding a blazed grating profile to the existing profile on the array, as is shown in (c) where the pattern of (a) has been steered out of the camera field. A more complex fanout is shown in (d), where two rows and two columns

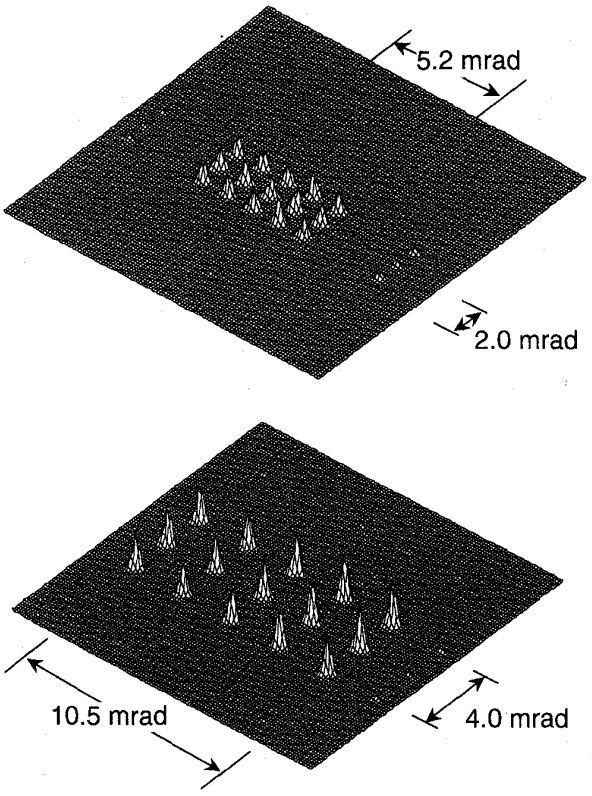

Fig. 25. 3 × 5 beam fanout with adjusted fanout spacing.

have been deleted. With the current device architecture, fanout patterns are limited to those which are separable in Cartesian coordinates.

The maximum aperture size of these optical phased arrays is limited by the wafer-size handling limits of the semiconductor-like processing equipment required for fabrication. Current devices have clear apertures as large as 4 cm. The technology for fabricating 10-cm units is under development. Apertures larger than 10 cm will eventually be available either through the use of state-of-the-art processing equipment, or by the mosaic tiling of multiple, smaller, apertures. The fabrication technology is based on well known semiconductor lithography and liquid crystal display technology; consequently, the potential is high for very low-cost, high-volume implementation.

Successful operation of these optical phased arrays in coherent laser radars has been demonstrated both at Wright Laboratories and at Raytheon. The heterodyne efficiency of a laser radar is a sensitive function of beam aberration. Measurements using existing carbon dioxide (10.6 μm) and doubled Nd:YAG (0.53 μm) laser radars demonstrated no measurable degradation of heterodyne efficiency when the optical phased arrays were used to steer the transmit/receive beams; the uncertainties of the measurements were approximately $\pm$ 0.5 dB. No anomalies were observable with either system. A demonstration using a 1.06 μm fiber-coupled laser radar system at Wright Laboratories [60] showed unexpected sidelobes 1 kHz off the Doppler return signal and about 30 dB down. This was found to arise from the 1 kHz sinusoidal drive for the liquid crystal phase shifters which imposed a small residual FM phase modulation on the steered beam. Subsequent operation of the phased array with square wave excitation effectively eliminated the sidelobes, as predicted. The sidelobes corresponded to velocities on the order of several millimeters per second and were therefore quite insignificant. Nevertheless, for sensitive measurements, this artifact is easily removed.

Properly designed liquid-crystal-based devices are capable of handling high peak input fluences and even relatively high average powers. Laser damage thresholds for a number of commercially available liquid crystals have been measured [61] at the University of Rochester prior to their use in components for the Omega fusion facility. The short-pulse (1 ns) fluence damage threshold for E7 was found to be 15.1 ± 1.7 J/cm^2 at 1.053 μm wavelength (one on one). N-on-one thresholds, in which a number of pulses are used prior to determining damage threshold, were found to be about one-half this level. Similar damage thresholds were found for other common liquid crystals. It should be noted, however, that achieving these damage threshold levels requires the use of particulate-free liquid crystals.

Optical field induced reorientation of the liquid crystal director can occur if the field intensity is high enough. The resultant phase shift could, in principle, degrade the steering efficiency of an optical phased array; however, this effect has not proven problematic to date. A considerable literature base is available to describe the optical reorientation effect, which has been used to realize highly nonlinear optical devices [62]. The amount of induced reorientation (and the resultant phase shift) depends on the intensity and pulse duration of the beam and the thickness of the liquid crystal layer. Typically a relatively thick liquid crystal layer (50–100 μm) is used and the input beam is focused to achieve multiple MW/cm^2 intensities in order to observe the effect. These are not typical operating conditions for a phased array used for sensor applications. Because a phased array is usually operated with the input beam deliberately spread over a relatively large aperture in order to obtain a small far-field spot size, such high intensity levels are not generally reached. Even for a case of high peak intensity, the reorientation from a single pulse is generally small. Using Khoos model, we estimate that a 10 ns pulse at 100 MW/cm^2 would induce only about 2 mrad of phase shift in a 3 μm thick layer of E7 liquid crystal (typical for an optical phased array for operation in the visible). This level of phase deviation is smaller than the least significant phase adjustment possible with the current driver electronics, and is not significant for operation of the phased array. Furthermore, the optically induced phase shift decays at the response time of the device; thus for laser pulse repetition rates less than the agile switching rate, the optically induced phase errors cannot accumulate pulse-to-pulse. However, higher intensities and longer pulses will induce proportionally larger phase shifts, and higher PRF's will allow pulse-to-pulse accumulation; under these conditions the applicability of a liquid-crystal based phased array

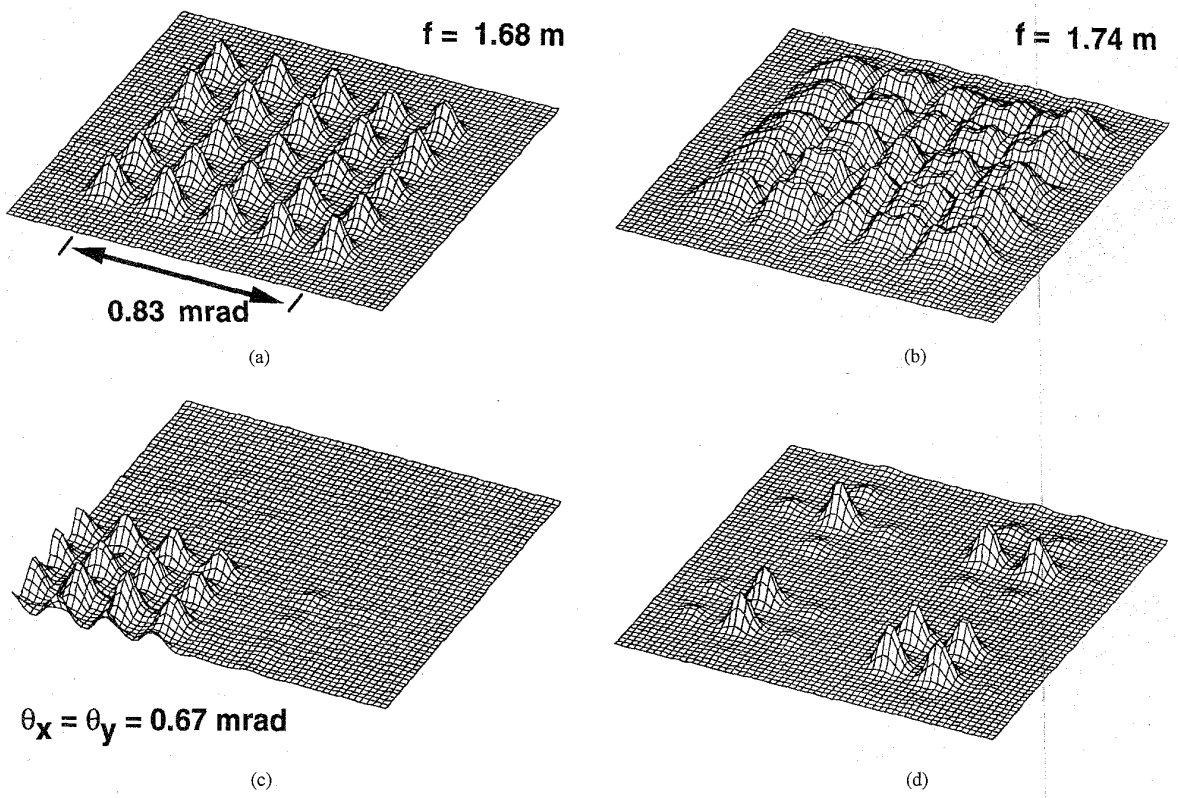

Fig. 26. 5 × 5 fanout, with focus/defocus.

must be carefully considered. Continuous wave operation represents the worst case for optical reorientation effects. Only limited data are available for this case; however, an electrically tunable half-wave plate using E7 liquid crystal has been demonstrated to operate without measurable field reorientation for input field intensities at least as high as 900 W/cm^2 at 10.6 μm wavelength [63].

With large area beams, it is thought that beam-induced thermal effects will generally determine the operational limits of a liquid crystal device. In the above CW experiments it was demonstrated that the device performance is driven by simple thermal effects. Absorption of the beam by the liquid crystal will raise its temperature; if it rises above the isotropic-nematic clearing temperature, the birefringence disappears and the device ceases to operate. This is generally a graceful failure mode. As the temperature rises, the birefringence monotonically decreases. If the temperature rise is uniform and is monitored, the decreasing phase shifts can be fully compensated with higher drive voltages, until the isotropic-nematic clearing temperature is reached. When subsequently cooled to a temperature less than the clearing temperature, operation automatically resumes. If the liquid crystal layer heats nonuniformly, as is the usual case for Gaussian beams, aberrations may be induced in the beam, as is well understood from the literature of optical windows. Uniform illumination produces no aberration. The formalism established by Klein [64] for face-cooled and edge-cooled Faraday rotators can be directly applied to liquid crystal phased arrays. With the exception of small amounts of defocus, spherical aberration is found to be the primary thermally induced error, and it depends linearly on the average power of the incident beam. Depending on device design, materials used, and the incident beam profile, modeling indicates that average powers ranging from a few kW to several MW could be handled by devices of 10 cm aperture with Strehl ratio no less than 0.8.

VI. Steering Passive Acquisition Sensors

In many implementations of a laser radar, an acquisition sensor is required to provide coarse target direction estimates. The pointing of the laser radar is then cued by the acquisition sensor. Because the field of view (FOV) of a laser radar system can be many orders of magnitude smaller than the FOV of a passive staring array, it is desirable to have as many sample points across the acquisition sensor FOV as possible. A large number of sample points across the acquisition sensor FOV can either be obtained by a single stage with a large number of sample points, or by a two stage process, with initial course sampling, followed by a narrow FOV steereable sensor with very high sampling angular resolution. One method to increase the sampling across an entire FOV is microscanning, discussed below [65].

If a two stage acquisition approach is used, it is necessary to steer an entire high resolution, narrow FOV passive

sensor anywhere in the FOV of a course resolution passive acquisition sensor. The difficulty in large angle, high resolution steering of broad spectral band radiation with liquid crystal phased arrays is that the 2π phase reset is correct at only a single wavelength. All subsequent sub arrays will have an incorrect phase shift except at the design wavelength. Fig. 3 shows that the average slope of the unfolded phase line is different for each wavelength, so energy at wavelengths other than the design wavelength is steered to a different angle. If it were possible to make a thick enough liquid crystal layer so that no phase resets were required, then we would have a nondispersive broadband beam steering system. In microwave phased array systems this is referred to as true time delay. Due to time response considerations discussed above, fringing field problems [8], and alignment layer difficulties in the liquid crystal, it is not currently possible to make large angle, large aperture beam steerers unless resets are used. Therefore we do not have true time delay, and dispersion will cause image degradations in optical systems which steer high resolution, broadband radiation through large angles.

In microscanning several images of the object are recorded, with the field-of-view of the detector array being shifted by a fraction of a detector element spacing between each recorded image [61]. The field-of-view is not moved while the image is recorded. Consider a detector sampling array as illustrated in Fig. 27. In normal operation, each element in the detector array would view a fixed portion of the object, as illustrated in Fig. 27(a). In a microscan operation, successive images are recorded at each of the shifted image positions, as illustrated in Fig. 27(b)–(d). In this example, the images are shifted by half a detector pitch at a time. The collection of images are then combined to produce a single image, with increased spatial sampling. The sampling at higher spatial frequencies reduces aliasing. A typical microscan architecture is to use four image samples to generate one image frame. Since the required angular motion between image samples is very small, it is possible that the liquid crystal beam steerer will not require phase resets across the aperture and therefore will not reduce image quality due to dispersion. This type of operation has been demonstrated using liquid crystal optical phased arrays [66]. We consider a sensor with the parameters listed in Table 2. Based on the values in Table 2, we see that the amount of microscan will be a fraction of the detector pitch, which is 60 μrad or 120 μrad, depending which spectral band is used. The largest angular movement is therefore 60 μrad for long-wave infrared (LWIR) and 30 μrad for middle-wave infrared (MWIR), assuming motion of half a pixel. It has been shown that smaller image shifts can be used to reconstruct images out to twice the Nyquist frequency imposed by the focal plane array [17]. Smaller image shifts require smaller steering angles and hence smaller OPD. Therefore, dispersionless beam steering is possible for these small angles because no resets will be required. Even if the beam steering element were placed in a location in the optical system with a smaller beam diameter, the same thickness of liquid crystal material would be required because the deflection angle needed at that location would be greater.

Some applications may require a large field-of-regard (FOR) as large as $30° \times 30°$ or even $60° \times 60°$. For such a large FOR, the need to microscan a staring array to increase the sampling rate becomes even more important because of limited angular sampling for practical array sizes. Table 3 gives potential sensor parameters for such an application. In this case resets probably will be required because the larger pixel spacing will imply larger steering angles, but the dispersion resulting from the resets may not be a limiting factor. The optical system specified in Table 3 would be very difficult to design, regardless of any dispersion issues, because of the speed of the optical system and the large image format. It is undesirable to curve the detector focal plane array, so field curvature will cause some image degradation. As an example of the speed of the optical system that would be required, consider a detector pitch of 100 μm. The detector angular subtense (DAS) would then be 1 mrad with 10 cm focal length optics. If the detector pitch were reduced to 50 μm, then a 5 cm focal length would be needed to keep the 1 mrad DAS. This in turn implies an F/0.5 system for a 10 cm aperture. A 20 cm aperture becomes totally unrealistic for a 5 cm focal length. Smaller aperture diameters would make the design problem easier, but the focal plane is still very large. The one saving feature to this sensor is that the DAS is only 1 mrad, so the optical system can depart significantly from the diffraction limit without causing a serious impact on image quality.

To microscan angles as large as 0.5 mrad (for a 1 mrad DAS) will require that the phase profile have resets across the aperture; therefore, dispersion will be an issue. The loss of image quality due to dispersion, however, may not be significant compared to the effects of the optics and the large detector size. The angle to which light of a different wavelength than the design wavelength is steered is given, for small angles, by [67]

$$\theta_\lambda = \theta_0 \frac{\lambda}{\lambda_0} \tag{19}$$

where θ_λ is the steered angle for wavelength λ and θ_0 is the steered angle at the for the design wavelength λ_0. From (19) it can be seen that even with a 4 μm bandwidth and a steering angle of 0.5 mrad, the spread of steered angles would only be from 400–600 μrad for a mean wavelength of 10 μm. For this example, the spread in angle is much less than the detector angular subtense.

We should note however the spread in angle predicted by (19) is only one aspect of dispersion. Another effect of dispersion is the creation of multiple sidelobes due to the many grating orders associated with a phased array [68]. Referring to Fig. 3, it can be seen that the unfolded phase for a wavelength different than the design wavelength is not continuous. Since the unfolded phase is not a straight line the steering efficiency will be affected. Energy will be directed to other allowed gratings modes of the optical

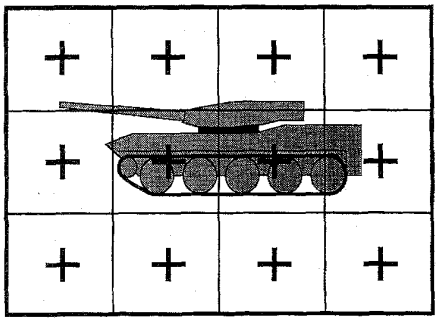

(a)

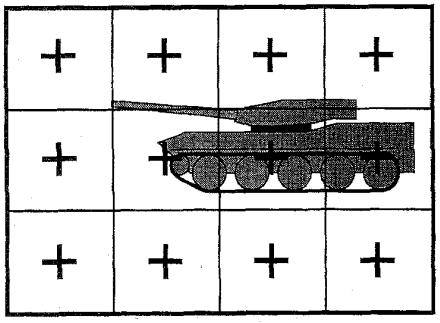

(b)

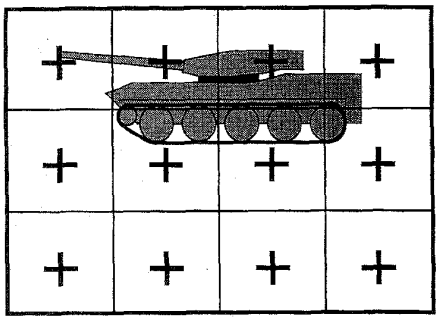

(c)

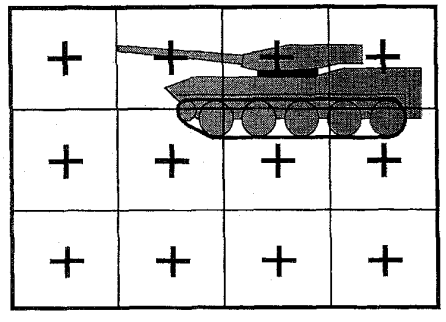

(d)

Fig. 27. Illustration of the microscan process. (a) Image of object superimposed on detector array. (b) Location of image with respect to detector array is shifted by half a pixel spacing in the horizontal direction. (c) Location of image is shifted by half a pixel spacing in the vertical direction. (d) Location of image is shifted by half a pixel spacing in both the horizontal and vertical directions. The effect of the microscan process is to increase the spatial sampling rate of the detector array, which can significantly reduce aliasing.

Table 2 Parameters of a Potential Sensor for Small Angle Microscan. The Detector Instantaneous Field-of-View is Matched to the Diffraction Limit of the Optical System

Detector array format	512 × 512
Pitch	50 μm
Detector array sizes	2.56 × 2.56 cm
Bands	4.3–5.3 μm (MWIR), 8.6–10.6 μm (LWIR)
Aperture diameter	20 cm
Diffraction limit	60 μm rad for MWIR, 120 μm rad for LWIR
Focal length	83.3 cm for MWIR, 41.7 cm for LWIR
Detector IFOV	60 μm rad for MWIR, 120 μm rad for LWIR
Total FOV	30 mrad (1.8°) for MWIR, 60 mrad (3.5°) for LWIR

Table 3 Parameters of a Potential Sensor for Large Angle Microscan. The Detector Instantaneous Field-of-view is Large (1 mrad) So That a Large Total Field Will Be Covered by the Sensor

Detector array format	512 × 512
Detector Pitch	100 μm
Detector array size	5.12 × 5.12 cm
Bands	4.3–5.3 μm or 8.6–10.6 μm
Aperture diameter	10 cm
Diffraction limit	117 μrad
Focal length	10 cm
Detector angular subtense	1 mrad
Total FOR	512 mrad (29.3°)

phased array, thus spreading the energy across various angles. If it were possible to find a liquid crystal with a birefringence Δn in the wavelength band of interest given by

$$\Delta n = \Delta n_0 \frac{\lambda}{\lambda_0} \tag{20}$$

where Δn_0 is the birefringence at the design wavelength, then the unfolded phase ramp would be a straight line. Each sub array would then have the correct phase shift at all wavelengths. However, even if such a liquid crystal could be fabricated, it may not have other desirable properties, such as fast response time and large birefringence. It also is likely to have absorption, since large dispersion in a medium tends to occur near absorption lines.

One method to decrease the difficulty of the optical design problem highlighted above is to limit the FOV of the sensor, then to use a steering mechanism to step the FOV through a larger FOR. As an example to highlight the tradeoffs involved, consider a sensor with a 256 × 256 element focal plan array and with an FOV of 100 mrad. The individual detector element IFOV is then approximately 400 μrad. The FOR is assumed to be 200 mrad so the entire sensor FOV must be step-scanned over an angle of 100 mrad. For steering angles on the order of 100 mrad and an aperture size of 10 cm, an OPD of 10 mm is required. A liquid crystal with birefringence of 0.2 would require a layer that is 25 mm thick (in the reflective mode), which would obviously be impractical. Therefore, 2π phase resets must be used to keep the liquid crystal thickness to realizable values.

Table 4 Comparison of a Step-stare and a Scanning Sensor. The Spectral Width for the Staring Sensor is Determined by the Resolution Required. The Center Wavelength for the Step-stare Sensor is 9.6 μm; the Steering Angle is 100 mrad. The Sensitivity Loss is Compared to a 3 μm Bandwidth. The Scanning Sensor is Assumed to Scan Over 480 Lines

Resolution	Spectral Width	Sensitivity Loss	Ratio of Signal Loss	Equivalent Number of Elements in TDI
60 μrad	.00576 μm	23	521	0.9
120 μrad	.0115 μm	16.1	260	1.8
250 μrad	.024 μm	11.2	125	3.85
500 μrad	.048 μm	7.9	62.5	7.7
1000 μrad	.096 μm	5.6	31.25	15.4
2500 μrad	.24 μm	3.54	12.5	38.4

As an example, we assume that the 2π phase resets are designed for a wavelength of 9.6 μm (for an 8.6–10.6 μm band). Using (19), we see that a point source emitting in the 8.6–10.6 μm band will be spread over a 20 mrad angle for steering of 100 mrad at 9.6 μm. This is over 85 times the diffraction limited angle of a 10 cm aperture. Therefore, an alternate approach must be used if we wish to steer passive radiation over a large angle with any accuracy, or one must be capable of digital post-detection compensation of a factor of 85. The most obvious method of steering passive radiation with a writable grating is to restrict the radiation to a narrow band, which reduces the amount of light incident on the detector. For shot-noise limited detection, the sensitivity of a sensor varies as the square root of the intensity of the incident light [69], and therefore as the square root of the spectral band width. As more energy is collected, the signal increases linearly while the shot noise increases only as the square root of the increase in collected energy. Changing the integration time of the detection process has the same effect as changing the spectral bandwidth of the light incident on the detector.

We can compare the effect of reducing the spectral bandwidth of the light incident on a staring sensor to the effect of reduced integration time per pixel of a scanning sensor. Equation (19) can be rewritten to specify the spectral bandwidth Dl that will allow a desired angular spread $\Delta\theta$:

$$\Delta\lambda = \frac{\Delta\theta}{\theta_0}\lambda_0. \tag{21}$$

We use (21) to calculate the spectral width associated with a specified angular spread. The results are presented in Table 4. If an 8–11 μm bandwidth is assumed, then 3 μrad divided by the allowed spectral width will yield the relative loss of signal strength for a sensor that uses only the allowed spectral bandwidth. The square root of that value will be the reduction in sensitivity. Note that in this simple example we are neglecting many factors, such as detector responsivity as a function of wavelength and the effect of spatial noise.

The last column in Table 4 is used to compare a dispersive nonmechanically scanned step-stare sensor with a mechanically scanned sensor that employs a linear array with multiple elements in time delay integration (TDI). The step-stare will make use of a limited bandwidth because of dispersion, while the scanning sensor will have decreased integration time because each detector element must scan over a number of pixels. The last column in Table 4 gives the equivalent number of detector elements in TDI that an 8–11 μm bandwidth scanning sensor must have to achieve the same sensitivity as a staring sensor with the spectral bandwidth (centered on 9.6 μm wavelength) given in the second column. It is assumed that each detector in the linear scanning sensor views 480 pixels. Table 4 shows that in this example, for a scanning sensor with four or less elements in TDI, the equivalent spectral bandwidth of a step-stare sensor is small enough that the dispersion produced by the liquid crystal beam steerer is less than the IFOV of a detector element.

Reduction in signal strength is not necessarily a severe limitation for staring sensors because they typically have limited capacity to store the photoelectrons generated by the detector. In fact, some staring sensors limit the spectral bandwidth in order to limit the stored signal. For current detector technology, the bandwidth limitations stated above will not be restrictive if a high quantum efficiency staring sensor is used. As charge storage capabilities improve, or as focal plan read-out rates increase, some method of dispersion compensation must be employed to make use of the larger allowed signal level, which we now consider.

Achromatic, all-diffractive systems have been considered in the literature, and paraxial designs have been developed which correct for dispersion [70]. Such approaches are difficult to implement in an optical system that employs a writable grating because the grating period of the active element is constantly changing. The most direct method to compensate for the dispersion of the active element is to have a second, writable optical element with dispersion opposite to that of the beam steering element. A second beam steering element can compensate for the dynamic dispersion, but designs we have investigated to date also eliminate the steering of the first element. Other approaches to correct the dispersion of the writable element include the use of fixed-period gratings or of refractive components. The use of fixed-period gratings in the system will retain the steering properties of the system and will correct for the dispersion at a particular angle, but will not correct the dispersion at all steering angles. The use of refractive elements, which have dispersion that is opposite in sign to diffractive elements, in combination with diffractive elements has been considered in the literature [71], [72]. However, the magnitude of the dispersion produced by

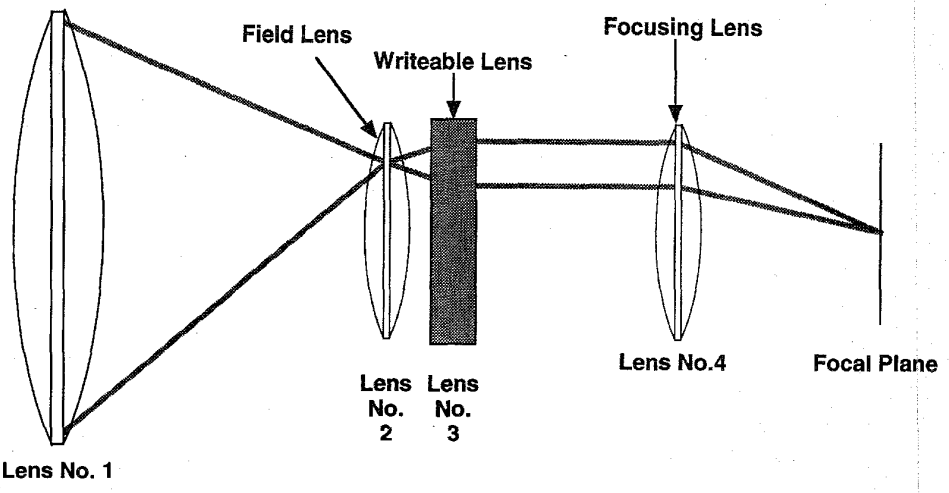

Fig. 28. *Broadband beam steering concept.* The first lens forms a large-format image at the second lens. The second lens makes the chief ray parallel to the optic axis. The third element is a writable lens. Its lateral location selects which portion of the image at the second lens is relayed to the focal plane. If the lens can be constructed without any phase resets, then it will not have dispersion.

diffractive elements is much greater than the dispersion produced by refractive elements. A combination of several of these approaches may lead to achromatic, diffractive beam steering systems, but more work is required to achieve practical designs.

A method to compensate for the dispersion is to use post-detection image processing [73]. If the spectrum of the incoming radiation is known, then an estimate of the chromatic point spread function can be obtained and the blur removed using a deconvolution scheme. A potential difficulty with post-detection processing alone is that the signal-to-noise ratio may be degraded because the received energy is spread over a large area in the image. It is likely that post-detection processing will be combined with optical correction approaches which correct some of the dispersion, to preserve the signal-to-noise ratio.

A different approach to the beam steering problem is illustrated in Fig. 28. In this concept, dynamic gratings are not used to steer the optical beam. Rather, a dynamic device is used to select a portion of a FOR to be relayed to the detector. In Fig. 28, the first lens forms an image of a wide FOR. The second lens is a field lens, which makes the system telecentric in image space. The third lens is a writable lens. Its placement in the plane of the liquid crystal device determines the angles in object space that are mapped on to the detector. The writable lens relays the image created by the first lens to infinity. The fourth lens creates a real image at the detector plane for all locations of the writable third lens. There are several design challenges with this approach to beam steering. One challenge is that the first lens must form a flat image over a very large format. The design will become more difficult as the steering angles become larger and resolution requirements increase. The second problem is that the writable lens may require a large OPD. If phase resets must be used, then the lens will be dispersive and therefore will have a different focal length for each wavelength of incident light. For a small enough lens diameter, it is possible to write a stair-step approximation to the desired lens shape without phase resets. The maximum OPD that a lens must have can be determined under the assumption of a parabolic profile [74]:

$$\mathrm{OPD}_{\max} = \frac{(D/2)^2}{2f} \tag{23}$$

where D is the diameter of the writable lens and f is the focal length of the lens. If we assume that the f-number of the writable lens is matched to the f-number of the first lens (which is taken to be $f/1$), then the maximum OPD is simply given by $D/8$. The diameter of the writable lens determines the FOV of the sensor; in other words, the lens diameter determines how much of the image at Lens 2 is relayed to the final image plane, and with how much vignetting. We will define the points in the image which experience 50% vignetting as the edges of the FOV. Table 5 lists the required lens diameter and required OPD for several possible values of FOV. As can be seen, the FOV associated with an OPD less than one wavelength is quite small. However, there may be potential applications for a sensor with such a small FOV. For example, a wide FOV passive sensor could be used to cue a steerable narrow FOV passive sensor with larger magnification.

Table 5 OPD Required For a Dispersionless, Writable Lens. The Diameter of the Lens is Determined by the 50% Vignetting Points in the Field-of-view

FOV	Diameter	Maximum OPD
0.25 mrad	200 μm	6.3 μm
0.5 mrad	300 μm	12.5 μm
1 mrad	450 μm	25 μm
2 mrad	700 μm	50 μm

VII. Laser Radar Systems Concepts

A number of electro-optic imaging systems could employ optical phased array technology. We highlight here a few system concepts.

A. Scanning Laser Radar Search Sensor

In this concept, no passive acquisition sensor would be required. Instead, a laser would be scanned over the field of regard to form an image over time. The beam steerer must be capable of directing the laser over the entire field of regard in a scanning manner. A random pointing capability is of secondary importance. In this concept the field of regard can be quite wide, so high steering efficiency at large angles is critical, or else the image quality may be affected [75].

B. Cued, High Resolution Imaging Laser Radar

This sensor suite would have a FOV covered by an unsteered staring infrared focal plane array. The staring infrared focal plane array would have sufficient resolution to hand over the spatial coordinates of interest to a laser radar. The laser radar would be steered over the acquisition sensor FOV by an optical phased array. The phased array would also provide small-angle stabilization. The acquisition sensor and the laser radar could be co-boresighted through a single aperture.

C. Enhanced Field of View Acquisition Sensor with Cued Laser Radar

The FOV of the acquisition sensor would be increased by microscanning the image on the passive focal plane array. The microscan process could be implemented with phased array beam steering technology. As discussed in Section III, a microscan implementation need not have dispersion if small image shifts are used. If larger image shifts are required, either because of noise [76] or the requirement to go to multiple microscan steps, dispersion may become an issue. In such an implementation it may be necessary to use digital post-detection processing to compensate for the effects of dispersion.

D. Agile Steered Acquisition Sensor FOV with Cued Laser Radar

In this concept, the passive acquisition sensor is steered by the phased array beam steerer. Digital post processing, or other similar approaches, will be needed to compensate for the dispersion produced by the beam steerer. The effect of dispersion on the image quality could be reduced by the use of large pixels, which would however limit the handover accuracy to the laser radar and therefore decrease its range.

E. Two Stage Passive Sensor and Cued Laser Radar

The first stage of this concept would be a large FOV passive staring acquisition sensor with coarse resolution (possibly microscanned). The second stage would be a narrow FOV passive sensor using the FOV steering concept described in Fig. 28. If the FOV of the second stage passive sensor is kept small, then a writable lens need have no dispersion. The resolution of this second stage would hand over to a laser radar with sufficient accuracy so that the laser beam would not need to be spoiled. The laser radar would be steered by an optical phased array for both agile pointing as well as fine stabilization.

VIII. Conclusions

There are limited options for steering optical sensors without using mechanical motion. Liquid-crystal-based optical phased arrays are now becoming available and represent a promising option for realization of true non-mechanical beam steering. Optical phased arrays are ideal for steering monochromatic laser radar beams. They will greatly simplify beam stabilization as well as pointing, resulting in a much lower cost for high performance, stabilized optical sensors. Dynamic focus/defocus has been demonstrated, as has been programmable multiple beam fanouts. Concepts have been developed to apply optical phased array technology to laser radars and to their passive acquisition sensors. A potential near-term application of phased array technology in passive acquisition sensors is microscanning. Large angle scanning of passive acquisition sensors can be accomplished using optical phased arrays if the spectral bandwidth is restricted. If these sensors employ high quantum efficiency detectors, the net system sensitivity can be similar to state-of-the art scanning sensors. Dramatic cost savings for high performance laser radars will occur as optical phased array technology becomes available. Performance increases will be possible through the use of rapid random access pointing anywhere in the FOV, simple fine stabilization, and dynamic focus/defocus control. Future growth areas include adaptive optics wavefront correction and atmospheric compensation, and enhanced optical pattern recognition utilizing phase templates on either the transmit and/or the received beam. For the performance improvements of existing optical sensor systems as well as for the enabling of entirely new sensor systems, optical phased array technology is expected to have a revolutionary impact on electro-optical systems.

References

[1] R. A. Meyer, "Optical beam steering using a multichannel lithium tantalate crystal," *Appl. Opt.*, vol. 11, pp. 613–616, Mar. 1972.

[2] Y. Ninomiya, "Ultrahigh resolving electrooptic prism array light deflectors," *IEEE J. Quant. Electron.*, vol. 9, pp. 791–795, Aug. 1973.

[3] A. Tanone, Z. Zhang, C.-M. Uang, and F. T. S. Yu, *Microwave and Opt. Technol. Lett.*, vol. 7, pp. 285–289, Apr. 1994.

[4] F. Vasey, F. K. Reinhart, R. Houdré, and J. M. Stauffer, "Spatial optical beam steering with an AlGaAs integrated phased array," *Appl. Opt.*, vol. 32, pp. 3220–3232, June 1993.

[5] R. M. Matic, "Blazed phase liquid crystal beam steering," *Laser Beam Propagat. and Contr.: Proc. Soc. Photo Opt. Instrum. Eng.*, vol. 2120, pp. 194–205, 1994.

[6] T. A. Dorschner *et al.,* "Liquid crystal beam steering; an optical phased array for lasers," presented at the *1991 Meet. IRIS Specialty Group on Active Syst.,* Oct. 1991.
[7] P. F. McManamon and T. A. Dorschner, "Space fed optical phased arrays and their applications," presented at the *1993 Meet. IRIS Specialty Group on Active Syst.,* Nov. 1993.
[8] T. A. Dorschner, D. P. Resler, D. S. Hobbs, and R. C. Sharp, "Phased array beam steering of long-wave infrared lasers," to be published in *Opt. Lett.*
[9] T. A. Dorschner *et al.,* "Optical phased array beam steering at 1.06 microns," to be published in *Opt. Lett.*
[10] M. I. Skolnik, *Introduction to Radar Systems.* New York: McGraw-Hill, 1962.
[11] J.-P. Huignard, M. Malard, and G. de Corlieu, "Static deflector device for an infrared beam," US Pat. No. 4,639,091, May 1987.
[12] H. Dammann, "Blazed synthetic phase-only holograms," *Optik,* vol. 31, pp. 95–104, 1970.
[13] R. A. Soref and M. J. Rafuse, "Electrically controlled birefringence of thin nematic films," *J. Appl. Phys.,* vol. 43, no. 5, pp. 2029–2036, 1972.
[14] P. F. McManamon, E. A. Watson, T. A. Dorschner, and L. J. Barnes, "Applications look at the use of liquid crystal writeable gratings for steering passive radiation," *Opt. Eng.,* vol. 32, no. 11, pp. 2657–2664, Nov. 1993.
[15] T. A. Dorschner *et al.,* Raytheon Co., private commun. (Beam Agility Techn. Final Rep., WL-TR-93-1020, 1993).
[16] T. C. Cheston and J. Frank, "Phased array radar antennas," in *Radar Handbook,* M. I. Skolnik, Ed. New York: McGraw-Hill, 1990, chapt. 7.
[17] G. D. Love, J. S. Fender, and S. R. Restaino, "Adaptive wavefront shaping with liquid crystals," *Opt. Photon. News,* pp. 16–21, Oct. 1995.
[18] R. Q. Fugate, "Laser beacon adaptive optics," *Opt. Photon. News,* pp. 14–19, June 1993.
[19] W. Goltsos and M. Holz, "Agile beam steering using binary optics microlens arrays," *Opt. Eng.* vol. 11, no. 29, pp. 1392–1397, 1990.
[20] T. D. Milster and J. N. Wong, "Modeling and measurement of a micro-optic beam deflector," *SPIE,* vol. 1625, 1992.
[21] E. A. Watson, "Analysis of beam steering with decentered microlens arrays," *Opt. Eng.,* Vol. 32, pp. 2665–2670, Nov. 1993.
[22] T. H. Lin, "Implementation and characterization of a flexure-beam micro mechanical spatial light modulator," *Opt. Eng.,* vol. 33, no. 11, pp. 3643–3648, 1994.
[23] V. Bright, Air Force Inst. Technol., private commun.
[24] A. Yariv, *Introduction to Optical Electronics.* New York: Holt, Rinehart and Winston, 1971, chapt. 9 and 12.
[25] I. P. Kaminow, *An Introduction to Electrooptic Devices.* Orlando, FL: Academic, 1974.
[26] M. Gottlieb, C. L. M. Ireland, and J. M. Ley, *Electro-Optic and Acousto-Optic Scanning and Deflection.* New York: Dekker, 1983.
[27] L. Beiser, *Laser Scanning and Recording.* Bellingham, WA: SPIE, 1985, vol. 378.
[28] G. F. Marshall, *Optical Scanning.* New York: Dekker, 1991.
[29] J. Dougherty *et al.,* "Rapid optical beam steering sensor suite for tactical weapon tracking applications," in *Laser Beam Propagation and Control,* H. Weichel and L. F. DeSandre, Eds. Bellingham, WA: SPIE, 1994, vol. 2120, pp. 211–217.
[30] B. D. Nordwall, "Russian innovation offers affordable phased array," *Aviation Week,* Apr. 1995, p. 69.
[31] E. Brookner, "Fundamentals of radar design" in *Radar Technology.* Dedham, MA: Artech, 1977, pp. 26–36.
[32] L. Beiser, "Laser beam information scanning and recording," in *Laser Scanning and Recording.* Bellingham, WA: SPIE, vol. 378, pp. 3–24, 1985.
[33] S. D. Jacobs, "Liquid crystals for laser applications," in *CRC Handbook of Laser Science and Technology.* vol. 4, M. J. Weber, Ed. New York: CRC, 1986.
[34] L. M. Blinov, *Electro-optical and magneto-optical properties of liquid crystals.* Chichester, UK: Wiley, p. 292, 1983.
[35] S.-T. Wu, A. M. Lackner, and U. Efron, "Optimal operation temperature of liquid crystal modulators," *Appl. Opt.,* vol. 26, pp. 3441–3445, 1987.
[36] S.-T. Wu, U. Finkenzeller, and V. Reiffenrath, "Physical properties of diphenyl-diacetylenic liquid crystals," *J. Appl. Phys.,* vol. 65, pp. 4372, 1989.
[37] S-T. Wu and C. S. Wu, "Experimental confirmation of the Osipov-Teretjev theory on the viscosity of nematic liquid crystals," *Phys. Rev. A,* vol. 42, no. 4, pp. 2219–2227, 1990.
[38] G. Sharp and K. Johnson, "High speed analog complex-amplitude liquid crystal light modulator," *Optics Lett.,* vol. 19, no. 16, Aug. 1994.
[39] S.-T. Wu, "Room temperature diphenyl-diacetylene liquid crystals," *Appl. Phys. Lett.,* vol. 61, pp. 630, Aug. 1992.
[40] D. MacDonnel, Defense Res. Estab., Malverne, UK, private commun.
[41] P. Yeh, *Optical Waves in Layered Media.* New York: Wiley, 1988, p. 150.
[42] M Sansone *et al.,* "Large Kerr effects in transparent encapsulated liquid crystals," *J. Appl. Phys.* vol. 67, no. 9, May 1990.
[43] T. A. Dorschner, "Optical phased array beam steerer including prism," US Pat. 5,018,835, May 1991.
[44] S. A. Serati, G. D. Sharp, and R. A. Serati, "128 × 128 analog liquid crystal spatial light modulator," in *Opt. Patt. Recog. VI,* SPIE, vol. 2490, pp. 378–387, 1995.
[45] K. M. Johnson *et al.,* "Chiral smectic liquid crystals for high information content displays and spatial light modulators," in *Tech. Dig. Topical Meet. on Spatial Light Modulators and Applic.,* Washington, DC: Opt. Soc. Amer., 1993, pp. 18–21.
[46] G. D. Sharp, Boulder Nonlinear Corp., private commun.
[47] D. P. Resler, "Liquid crystal window," US Pat. No. 4,882,235, Nov. 1989.
[48] T. A. Dorschner and D. P. Resler, "Deflector for an optical beam," US Pat. No. 4,964,701, Oct. 1990.
[49] T. A. Dorschner, "Optical beam steerer having subaperture addressing," US Pat. No. 5,093,740, Mar. 1992.
[50] ——, "Method for providing beam steering in a subaperture-addressed optical beam steerer," US Pat. No. 5,093,747, Mar. 1992.
[51] S. T. Kowel, P. Kornreich, and A. Nouhi, "Adaptive spherical lens," *Appl. Phys. Lett.,* vol. 23, pp. 2774–2777, Aug. 1984.
[52] B. J. Cassarly, J. C. Ehlert, and D. J. Henry, "Low insertion loss high precision liquid crystal optical phased array," *Proc. Soc. Photo Opt. Instrum. Eng.: Free-Space Laser Commun. Technol. III,* vol. 1417, pp. 110–121, 1991.
[53] L. J. Friedman *et al.,* "Phase imaging a programmable liquid crystal grating," submitted to *Appl. Opt.*
[54] W. H. Press, B. P. Flannery, S. A. Teukolsky, and W. T. Vetterling, *Numerical Receipes in C.* New York: Cambridge, 1988, pp. 343–352.
[55] H. Dammann and K. Gortler, "High efficiency in-line multiple imaging by means of multiple phase holograms," *Opt. Commun.,* vol. 3, pp. 312–315, 1971.
[56] U. Killat, G. Rabe, and W. Rave, "Binary phase gratings for star couplers with high splitting ratio," *Fiber and Integrated Opt.,* vol. 4, pp. 159–167, 1982.
[57] A. Marrakchi and K. Rastani, "Free-space holographic grating interconnects," in *Photonic Switching and Interconnects,* A. Marrakchi, Ed. New York: Dekker, 1994, pp. 249–321.
[58] S. E. Broomfield, M. A. Neil, E. G. Paige, and G. G. Yang, "Programmable binary phase-only optical device based an ferroelectric liquid crystal SLM," *Electron. Lett.,* vol. 28, pp. 26–28, 1992.
[59] T. H. Barnes *et al.,* "Reconfigurable free-space optical interconnections with a phase-only liquid crystal spatial light modulator," *Appl. Opt.,* vol. 31, pp. 5527–5535, 1992.
[60] S. H. McCraken and M. S. Salisbury, "Coherent 1.06 micron system for liquid crystal beam steering evaluation," in *Proc. IRIS Specialty Group on Active Syst.,* Silver Springs, MD, 1991.
[61] S. D. Jacobs *et al.,* "Liquid-crystal laser optics: design, fabrication, and performance," *J. Opt. Soc. Amer. B,* vol. 5, no. 9, pp. 1962–1978, Sept. 1988.
[62] I. C. Khoo *et al.,* Ibid., and references therein.
[63] R. C. Sharp, D. P. Resler, D. S. Hobbs, and T. A. Dorschner, "Electrically tunable liquid crystal wave plate in the infrared," *Opt. Lett.,* vol. 15, no. 1, pp. 87–89, Jan. 1990.
[64] C. A. Klein and T. A. Dorschner, "Power handling capability of Faraday rotation isolators for CO_2 laser radars," *Appl. Opt.,* vol. 28, no. 5, pp. 904–914, Mar. 1989.
[65] G. C. Holst, *Electro-Optical Imaging System Performance.* Winter Park, FL: JCD, and SPIE Opt. Eng. Press, Bellingham, WA, 1995, chapt. 5.5 and 9.3.
[66] K. Barnard, E. Watson, and P. McManamon, "Nonmechanical microscanning using optical space-fed phased arrays," *Opt. Eng.,* vol. 33, no. 9, pp. 3063–3071, Sept. 1994.

[67] L. Myers, "Broadband beam steering with liquid crystal optical arrays," Wright Lab., private commun., WL/TR-92 1003, US Air Force, 1992.
[68] E. A. Watson, P. F. McManamon, L. J. Barnes, and A. Carney, "Application of dynamic gratings to broad spectral band beam steering," in *Laser Beam Propagation and Control,* H. Weichel and L. F. DeSandre, Eds.; *Proc. SPIE,* vol. 2120, pp. 178–185, 1994.
[69] R. W. Boyd, *Radiometry and the Detection of Optical Radiation.* New York: Wiley, 1983, chapt. 8.
[70] W. C. Sweatt, "Achromatic triplet using holographic optical elements," *Appl. Opt.,* vol. 16, no. 5, pp. 1390–1391, 1977.
[71] G. M. Morris, "Diffraction theory for an achromatic Fourier transformation," *Appl. Opt.,* vol. 20, no. 11, pp. 2017–2025, 1981.
[72] D. Falkis and G. M. Morris, "Broadband imaging with holographic lenses," *Opt. Eng.,* vol. 28, no. 6, pp. 592–598, 1989.
[73] R. J. Broessel, R. C. Hardie, and V. Dominic, "Image restoration in broadband field-of-view steering with a liquid crystal beam steerer," submitted to *Opt. Eng.*
[74] W. J. Smith, *Modern Optical Engineering.* New York: McGraw-Hill, 1990, chapt. 13.
[75] E. A. Watson and L. J. Barnes, "Optical design considerations for agile beam steering," in *Laser Beam Propagation and Control,* H. Weichel and L. F. DeSandre, Eds., *Proc. SPIE,* vol. 2120, 1994, pp. 186–193.
[76] K. J. Barnard and E. A. Watson, "Effects of spatial noise on submicroscan interpolation," submitted to *Opt. Eng.*

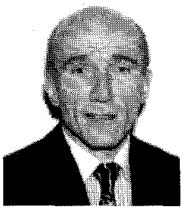

Paul F. McManamon (Senior Member, IEEE) received the Ph.D. degree in physics from Ohio State University in 1977.

He has been with Wright-Patterson Air Force Base since 1968, and he joined Wright Laboratory in 1979. His primary work since then has been in electro-optical sensors, including laser radar sensors and passive IR sensors. He is currently acting as Associate Chief Scientist for the Avionics Directorate at Wright Laboratories.

Dr. McManamon is a member of the Optical Society of America.

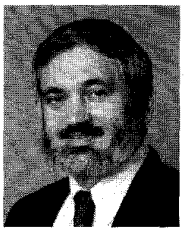

Terry A. Dorschner (Member, IEEE) received the B.S. degree in elelctrical engineering from the Massachusetts Institute of Technology, Cambridge, MA, in 1965, and the M.S. and Ph.D. degrees in electrical engineering from the University of Wisconsin at Madison in 1967 and 1971, respectively.

From 1971 to 1973, he was a Research Associate in the Institut für Hochfrequenztechnik at the Universität Brauschweig, Braunschweig, Germany, where he worked in the microwave and quasi-optical communications fields, extending the theory of multiple-state modulators, and developing a GHz semiconductor modulator for an experimental millimeter-wave communication system. He joined the Research Division of the Raytheon Company in 1974, where he invented and helped to develop a nonplanar laser gyroscope. In 1984, he was named Manager of the Electro-Optics Laboratory of the Research Division, in which he has overseen work on gaseous and solid-state lasers, nonlinear optical devices, isolators and modulators, integrated optics, and most recently, optical phased arrays. Since 1995 he has been Manager of Advanced Optics Technology for the newly formed Electronic Systems Division of Raytheon. He holds 20 US patents, has authored 17 scientific papers, and co-authored one book chapter.

Dr. Dorschner is a member of the Optical Society of America.

David L. Corkum received the B.S. degree in electrical engineering from the University of Massachusetts, Amherst, MA, in 1986, and the M.S. degree in electrical engineering from Northeastern University, Boston, MA, in 1991.

In 1991 he joined Raytheon's Research Division, where he has worked on infrared detectors and later electro-optics. Since 1995 he has worked in the Precision Controls Department of Texas Instruments, Inc., Attleboro, MA.

Larry Friedman (Member, IEEE) received the Ph.D. degree in experimental physics from Cornell University, Ithaca, NY.

From 1986 to 1989 he was a research faculty member in the University of Southern California's Physics Department, where he worked in the field of low temperature physics. Since 1989 he has been a Senior Scientist in the electro-optics group at Raytheon.

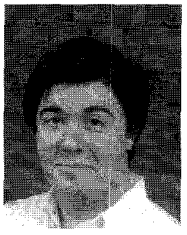

Douglas S. Hobbs received the B.S. degree in physics from Bucknell University, Lewisburg, PA, and the M.S. degree in electro-optics from Tufts University, Medford, MA, in 1985 and 1990, respectively.

He spent two years as a research scientist at the Corporate Research Center at Grumman Corporation, Bethpage, NY, where he worked on the development of multiple-focus holographic lenses for an optical pattern recognition system based on optical correlation. In 1987 he joined Raytheon's Research Division in Lexington, MA, where his research activities have included the development of holographic lithography techniques for patterning submicron-sized features over large areas. Additional interests have included the design and development of process technology for producing electro-optic laser beam steering devices, and the hardware and software design of electronic drivers for these devices. He holds two patents.

Mr. Hobbs is a member of the Optical Society of America.

Michael Holz (Member, IEEE) received the Diplom Physiker degree from the Technical University at Munich in 1974 and Ph.D. degree in physics from Massachusetts Insitute of Technology, Cambridge, MA, in 1978.

In 1978 he joined Raytheon Research Division, where he worked on perfecting the multi-oscillator ring laser gyroscope and helped with the transfer of this technology to Litton in 1985.

From 1985 to 1992 he was a staff member at MIT Lincoln Laboratory, where he worked on a variety of sensor technology issues with an emphasis on broadening the applications spectrum of binary optics. Since rejoining Raytheon in 1992, he has concentrated on developing commerical applications for Raytheon's optical phased array technology. He holds five US patents.

Dr. Holz is a member of Sigma Xi.

Sergey Liberman (Member, IEEE) received the M.S. degree in applied physics from St. Petersburg Polytechnic University, St. Petersburg, Russia, in 1982.

From 1989 to 1995 he was Research Scientist at Raytheonm where he was involved in the R&D of infrared photodetector arrays and agile laser beams steerers. He is presently an R&D scientist with SemiTest, Inc., where he works on the development of electro-optical characterization methods of semiconductor/insulator interfaces.

Huy Q. Nguyen received the B.S. degree in electrical engineering from Wentworth Institute of Technology, Boston, MA, in 1988. He received the M.S. degree in physics from the University of Massachusetts, Amherst, MA, in 1992.

He joined Raytheon in 1992, where his work included laser deposition of YBCO superconducting thin films and development of phosphors for field emission displays. His most recent work involved optical thin-film development for liquid crystal devices and interfacial layer growth for synthtic diamond films. He is presently with Koopin Corp., Taunton, MA.

Daniel P. Resler received the B.S. degree in materials science from Cornell University, Ithaca, NY, in 1980, and the M.S. degree from Northeastern University, Boston, MA, in 1985.

From 1980 to 1987 he was with Honeywell Corp., where he did process development and materials research on HgCdTe infrared detectors and materials. In 1987 he joined Raytheon's Research Division, where he is developing liquid crystal devices and technologies for liquid crystal device fabrication.

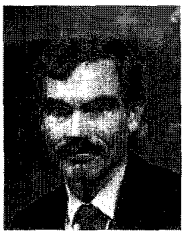

Richard C. Sharp (Associate Member, IEEE) received the B.S. degree in chemistry from the University of Florida, Gainesville, FL, in 1977, and the M.S. degree in chemistry and the Ph.D. degree in chemical physics from Harvard University, Cambridge, MA, in 1979 and 1982, respectively.

In 1982 he joined the Research Division of Raytheon Company, where he has worked for programs in lasers, electro-optics, and optoelectronics. He has developed homogeneous and heterogeneous catalysts for long-life sealed CO_2 lasers, diode-laser-driven 2 μm solid-state lasers, and optical parametric oscillators. He was responsible for the development of a passively mode-locked thulium fiber laser producing 190 femtosecond optical pulses.

Dr. Sharp is a member of the Optical Society of America and the American Physical Society.

Edward A. Watson received the B.S. degree in physics and the M.S. degree in optical sciences from the University of Arizona, Tucson, AZ, and the Ph.D. degree in optics from the University of Rochester, Rochester, NY.

He is an Electronics Engineer in the Electro-Optics Branch of Wright Laboratory at Wright Patterson Air Force Base. He is involved in research in active and passive electro-optic sensors, including the application of dynamic diffractive optical components to the agile steering of monochromatic and polychromatic light, and in the development of laser radar imaging sensors.